

Ocean Outgassing of Methyl Chloroform as an Underestimated Source of Emission

Peidong Wang¹, Susan Solomon², Jeffery R Scott¹, Shari Yvon-Lewis³, Paul O. Wennberg⁴, Ray F Weiss⁵, Matthew Rigby⁶, and Minde An¹

¹Massachusetts Institute of Technology

²Massachusetts Institute of Technology Department of Chemistry

³Texas A&M University

⁴California Institute of Technology

⁵University of California, San Diego

⁶University of Bristol

August 13, 2025

Abstract

Methyl chloroform (MCF) is a synthetic ozone-depleting substance used as an industrial solvent. Its primary sink is reaction with the hydroxyl radical (OH), making it a key tracer for estimating atmospheric oxidative capacity. Following Montreal Protocol regulations, MCF emissions declined rapidly after the 1990s. However, the recent slowdown in atmospheric MCF decay suggests persistent emissions and/or declining OH (contradicting chemistry-climate models projecting increasing OH). The air-sea exchange of MCF has been poorly constrained due to limited observations and simplified ocean representations. We simulate oceanic MCF fluxes using a modern ocean reanalysis and validate with depth-resolved observations. Results suggest the ocean has shifted from a net sink to a net source around 2005, outgassing 0.5 Gg yr⁻¹ in the 2010s (up to 30% of inferred MCF emissions). This ocean outgas is an order of magnitude larger than previous estimates and can have important implications for interpreting OH levels from MCF records.

1 **Ocean Outgassing of Methyl Chloroform as an Underestimated Source of Emission**

2

3 **Peidong Wang^{1*}, Susan Solomon¹, Jeffery R. Scott¹, Shari A. Yvon-Lewis², Paul O. Wennberg³,**
4 **Ray F. Weiss⁴, Matthew Rigby^{5,6}, Minde An⁶**

5

6 ¹Department of Earth, Atmospheric and Planetary Sciences, Massachusetts Institute of
7 Technology, Cambridge, MA, USA.

8 ²Department of Oceanography, Texas A&M University, College Station, TX, USA.

9 ³Division of Geological and Planetary Sciences, California Institute of Technology, Pasadena, CA,
10 USA.

11 ⁴Scripps Institution of Oceanography, University of California San Diego, La Jolla, CA, USA.

12 ⁵School of Chemistry, University of Bristol, Bristol, UK.

13 ⁶Center for Sustainability Science and Strategy, Massachusetts Institute of Technology,
14 Cambridge, MA, USA.

15

16 Corresponding author: Peidong Wang (pdwang@mit.edu)

17 **Key Points:**

- 18 • The ocean uptakes methyl chloroform (MCF) in the tropics and outgasses in the
19 extratropics, the reverse of many other tracers such as CFC-11
- 20 • Our model estimates that the ocean outgassed 0.5 Gg yr⁻¹ of MCF in the 2010s,
21 accounting for up to 30% of top-down inferred emissions
- 22 • This ocean outgassing is substantially larger than previous estimates and can
23 significantly affect inferred MCF emissions and OH levels
- 24

25 Abstract

26 Methyl chloroform (MCF) is a synthetic ozone-depleting substance used as an industrial solvent.
27 Its primary sink is reaction with the hydroxyl radical (OH), making it a key tracer for estimating
28 atmospheric oxidative capacity. Following Montreal Protocol regulations, MCF emissions
29 declined rapidly after the 1990s. However, the recent slowdown in atmospheric MCF decay
30 suggests persistent emissions and/or declining OH (contradicting chemistry-climate models
31 projecting increasing OH). The air-sea exchange of MCF has been poorly constrained due to
32 limited observations and simplified ocean representations. We simulate oceanic MCF fluxes
33 using a modern ocean reanalysis and validate with depth-resolved observations. Results
34 suggest the ocean has shifted from a net sink to a net source around 2005, outgassing 0.5 Gg yr^{-1}
35 in the 2010s (up to 30% of inferred MCF emissions). This ocean outgas is an order of
36 magnitude larger than previous estimates and can have important implications for interpreting
37 OH levels from MCF records.

38

39 Plain Language Summary

40 Methyl chloroform (MCF) is a human-made compound that depletes stratospheric ozone, and
41 its production has been phased out under the Montreal Protocol. However, recent observations
42 show that atmospheric MCF is declining more slowly than expected, suggesting the presence of
43 unexplained emissions and/or a decrease in hydroxyl radical (OH) levels (at odds with
44 chemistry-climate models that suggest OH should have remained stable or increased). As
45 anthropogenic MCF emissions have declined, the role of the ocean in both uptake and
46 outgassing of MCF has grown more significant, but this component has been largely overlooked
47 in previous studies. Here, we simulate ocean uptake and outgassing of MCF as accurately as
48 current constraints allow. We find that the global ocean likely shifted to a net source of
49 emission around 2005, releasing MCF at levels substantially higher than previously thought.
50 Global OH levels are typically inferred from measurements of atmospheric MCF, which is
51 primarily removed through reactions with OH, so changes in the MCF source strength in turn
52 imply changes in atmospheric OH, which may be as large as ~6% in the past few years. These
53 results highlight the importance of accurately representing air-sea exchange in atmospheric
54 trace gas budgets and inferences of OH levels.

55

56 1 Introduction

57 The hydroxyl radical (OH) is the primary atmospheric oxidant (Levy, 1971). OH governs
58 the lifetimes of key greenhouse gases including methane (McNorton et al., 2016; Prather et al.,
59 2012; Prather & Spivakovsky, 1990; Rigby et al., 2017; Turner et al., 2017) and various
60 halocarbons (Liang et al., 2017; Prather & Spivakovsky, 1990; Rigby et al., 2013) (e.g.,
61 hydrochlorofluorocarbons [HCFCs] and hydrofluorocarbons [HFCs]), and it also influences air
62 pollution through its role in tropospheric ozone chemistry (Levy, 1971; Singh et al., 1995).
63 Therefore, accurately characterizing atmospheric OH is crucial for estimating greenhouse gas
64 emissions as well as informing air pollution mitigation efforts. However, due to its extremely

65 short atmospheric lifetime of about one second, OH cannot be directly measured on a global
66 scale. Instead, global mean OH concentrations are most commonly inferred indirectly, from
67 observations of atmospheric methyl chloroform (CH_3CCl_3 ; MCF) (e.g., Krol & Lelieveld, 2003;
68 Montzka et al., 2011; Naus et al., 2019; Patra et al., 2014; Prather et al., 2012; Prinn et al., 1992;
69 Spivakovsky et al., 2000) — a relatively long-lived synthetic compound that has been globally
70 monitored since 1978 (Prinn et al., 2018) and is predominantly removed by reaction with OH.

71 However, critical yet unresolved discrepancies remain between OH levels inferred from
72 MCF using inverse modeling approaches and those simulated directly by process-based
73 chemistry-climate models based on known OH chemistry. Process-based chemistry-climate
74 models tend to overestimate absolute OH levels inferred from MCF by 10–15% (Naik et al.,
75 2013; Prather et al., 2012; Prinn et al., 2005). Chemistry-climate models also suggest stable or
76 slightly increasing OH (Stevenson et al., 2020; Zhu et al., 2024), which conflicts with some MCF
77 inverse modeling studies indicating a post-2005 decline (Rigby et al., 2017; Turner et al., 2017).
78 Although process-based OH levels show substantial spread across models (Murray et al., 2021;
79 Naik et al., 2013), MCF-based estimates can also carry large uncertainties and show differences
80 between studies, raising concerns about their continued reliability for the inference of global
81 OH (Nicely et al., 2020; Patra et al., 2021).

82 Inferring OH from MCF relies on knowledge of its source and sink terms. MCF is a
83 stratospheric ozone-depleting substance and its anthropogenic emissions have declined rapidly
84 due to controls of the Montreal Protocol (Laube & Tegtmeier, 2022). While bottom-up
85 inventories provide well-constrained MCF production and emission estimates prior to 2000
86 (McCulloch & Midgley, 2001), they have been poorly characterized in the years since. To
87 address this issue in quantifying OH, recent studies seek to simultaneously optimize both
88 anthropogenic MCF emissions and OH concentrations in joint inversions (e.g., Naus et al., 2021;
89 Rigby et al., 2017; Turner et al., 2017). However, other potential natural source and sink terms
90 for MCF (i.e., from ocean uptake and outgassing) are proportionally increasing their significance
91 as anthropogenic emissions have declined, introducing biases if these processes are poorly
92 represented or overlooked in the inversion. Studies have suggested unexplained emissions
93 occurring at least since 2013 (Naus et al., 2021; Rigby et al., 2017; Turner et al., 2017), when
94 global MCF consumption should have ceased (Rigby et al., 2017). A recent three-dimensional
95 model inversion further attributes these unexplained emissions primarily to high latitudes, and
96 suggested that the ocean could be a missing source (Naus et al., 2021).

97 Oceanic uptake and outgassing of MCF have been rather ambiguously represented in
98 previous OH inversions. MCF can dissolve in seawater and undergo further degradation through
99 hydrolysis (Butler et al., 1991; Gerkens & Franklin, 1989; Yvon-Lewis & Butler, 2002). Earlier
100 studies either neglect this process altogether or treat the ocean as a simple first-order loss term
101 (Patra et al., 2011, 2014; Prather et al., 2012; Turner et al., 2017). A more complex, time-
102 varying ocean uptake of MCF using an ocean general circulation model (Wennberg et al., 2004;
103 hereafter W04) has only been incorporated in OH inversion studies recently (Patra et al., 2021;
104 Rigby et al., 2017), and this oceanic term has been shown to be a dominant sensitivity factor for
105 inferred OH (Rigby et al., 2017). However, W04 extends their projections of MCF air-sea fluxes

106 beyond the 2000s, when atmospheric MCF observations were not available to constrain their
107 model. Moreover, W04 uses the freshwater solubility of MCF, which may overestimate
108 seawater uptake. Combined with limited ocean observations, their air-sea flux remains highly
109 uncertain (Naus et al., 2021; Wennberg et al., 2004) and appears insufficient to account for the
110 high-latitude source inferred in recent inversions (Naus et al., 2021; Rigby et al., 2017).

111 In this study, we simulate the ocean uptake and outgassing of MCF from 1992 to 2019
112 using the Estimating the Circulation and Climate of the Ocean (ECCO) framework (Forget et al.,
113 2015a), which provides a physically consistent, observationally-constrained reconstruction of
114 the global ocean. And by prescribing observed MCF atmospheric mole fractions from the
115 Advanced Global Atmospheric Gases Experiment (AGAGE) network (Prinn et al., 2018), the
116 model enables a realistic simulation of the oceanic uptake of MCF. A key strength of our study
117 is the validation of simulated MCF distributions using an extensive set of depth-resolved ocean
118 profile observations from a North Atlantic cruise conducted in July 2003 (A16N2003). We then
119 evaluate the magnitude of ECCO-simulated MCF ocean outgassing relative to inferred total
120 emissions, compare it with previous estimates, and discuss its potential implications for
121 inferred OH abundances.

122 **2 Materials and Methods**

123 2.1 Sampling during the A16N2003 cruise

124 Depth-resolved observations of CFC-11 and MCF were collected during the A16N2003
125 cruise aboard the National Oceanic and Atmospheric Administration (NOAA) R/V *Ronald H.*
126 *Brown*, during June to August in 2003. Nearly all simultaneous measurements of CFC-11 and
127 MCF were taken in July, spanning 44 stations from 45.5° N to 2° S along longitudes 20° W to
128 29° W. The cruise track is shown in Figure 1a insert panel with the red line. During this cruise,
129 over 600 data points were collected for each tracer, with maximum depth at ~5,900 m. Detailed
130 descriptions of the measurement and sampling techniques are provided in (Bullister & Gruber,
131 2012; Yvon-Lewis et al., 2004).

132 2.2 Ocean state estimate and atmospheric forcing

133 The ocean state is represented by ECCO Version 4 Release 5 (Forget et al., 2015a), which
134 assimilates satellite and in situ observations using the Massachusetts Institute of Technology
135 General Circulation Model (MITgcm; Marshall et al., 1997a, 1997b) to produce a physically
136 consistent ocean reanalysis from 1992 to 2019. The ECCO simulation is run on the Lat-Lon-Cap
137 90 (LLC90) grid, with a horizontal resolution of approximately 1°, 50 vertical layers extending to
138 ~6,100 m depth, and a time step of one hour. Modeled tracer concentrations and air-sea fluxes
139 outputs are archived as monthly means, gridded on a regular 1° × 1° horizontal grid from the
140 LLC90 grid.

141 We couple the ECCO ocean with monthly values of atmospheric mole fractions of CFC-
142 11 and MCF from the AGAGE 12-box model output (Rigby et al., 2013). This 12-box model uses
143 prior emission estimates for CFC-11 and MCF before 1978, and posterior emissions constrained

144 by AGAGE observations thereafter. As a result, it provides continuous monthly mole fractions
 145 for both species starting from a time when their atmospheric concentrations were effectively
 146 zero, allowing ocean accumulation to begin, and closely matches observations after 1978 (see
 147 Supplementary Figures S1 and S2 for CFC-11 and MCF, respectively). The lower tropospheric
 148 mole fractions are provided across four latitude bands: 30° N–90° N, 30° N–equator, equator–
 149 30° S, and 30° S–90° S. To estimate spatially continuous air-sea fluxes, we linearly interpolate
 150 the atmospheric mole fractions every 10° of latitude across the boundaries of adjacent latitude
 151 bands (i.e., linearly interpolate from 35° N to 25° N, 5° N to 5° S, and 25° S to 35° S).

152 Because ECCO simulates time-varying ocean states that closely reflect observations only
 153 after 1992, we use the 1992 ocean state as a fixed boundary condition to estimate the initial
 154 distributions of CFC-11 and MCF. Specifically, we repeat the 1992 forcing fields in ECCO while
 155 prescribing time-varying atmospheric mole fractions starting from 1951 for both CFC-11 and
 156 MCF, allowing for tracer uptake and accumulation over time. This approach yields a reasonable
 157 estimate of the initial tracer distribution in the ocean by 1992. All results presented in this study
 158 focus on the period from 1992 onward.

159 Detailed descriptions of MCF solubility and hydrolysis, as well as air-sea exchange
 160 parameterizations, are provided in the Supplementary Text.

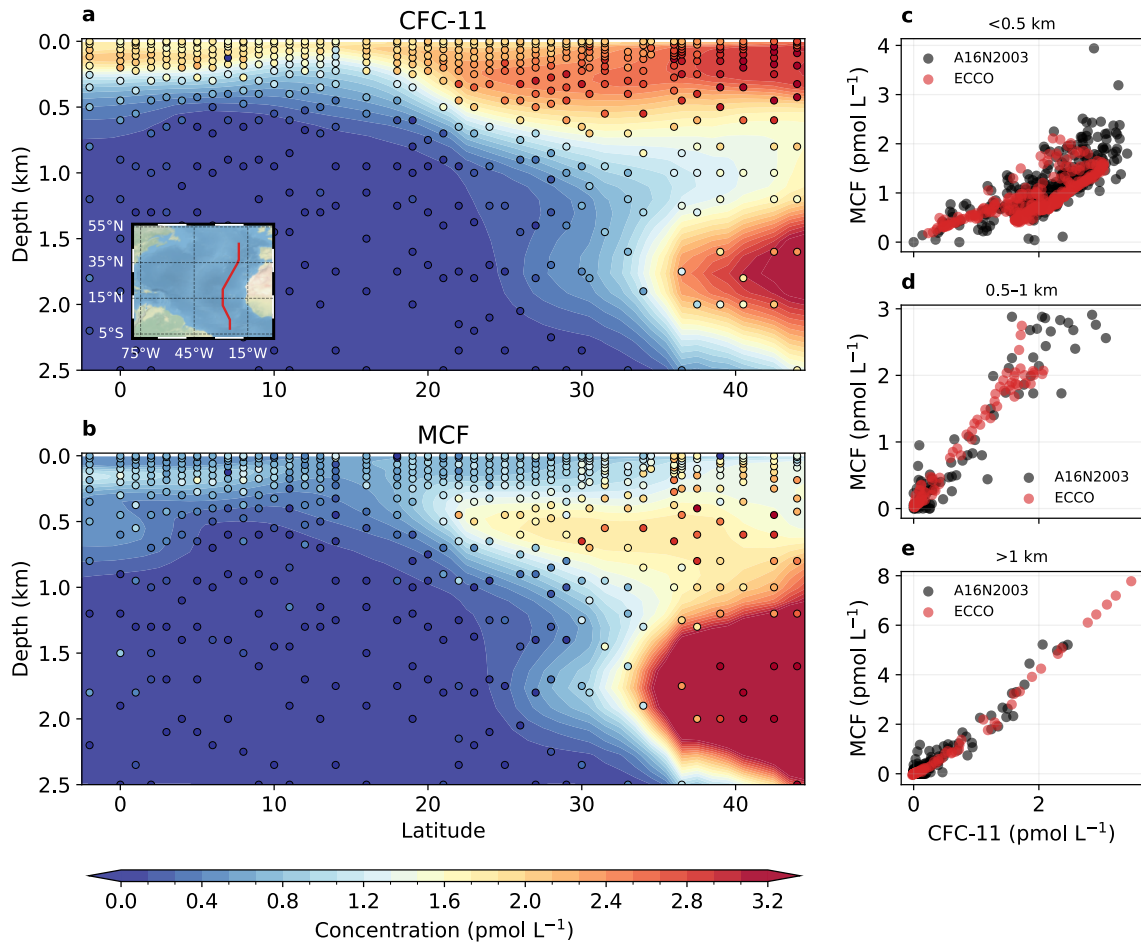
161 2.3 Quantifying changes in inferred OH associated with MCF air-sea fluxes

162 We estimate the amount of inferred OH required to account for the air-sea MCF fluxes
 163 using the following equation:

$$\frac{dB}{dt} \Big|_{ocn} = -k \cdot \Delta OH \cdot B \quad (1)$$

164 where B is the total atmospheric burden of MCF (in Gg, derived from observed atmospheric
 165 mole fractions [in parts per trillion; ppt] by applying a scaling factor of 23.57 Gg ppt⁻¹). This
 166 factor reflects the total atmospheric mass (5.1×10^{18} kg), along with the molar masses of air
 167 (28.96 g mol⁻¹) and MCF (133.4 g mol⁻¹). $\frac{dB}{dt} \Big|_{ocn}$ represents the rate of change in atmospheric
 168 MCF burden (in Gg yr⁻¹) due solely to air-sea exchange and is equivalent to the ocean uptake or
 169 outgassing of MCF. The reaction rate k corresponds to the temperature-dependent loss rate of
 170 MCF due to its reaction with OH, taken from Burkholder et al. (2019), assuming a mean
 171 tropospheric temperature of 266 K (as in Rigby et al., 2017). ΔOH represents the change in
 172 inferred OH that would be needed to account for the ocean-driven changes in atmospheric MCF
 173 burden. This approach requires only the total atmospheric MCF burden (can be derived from

174 observations) and the air-sea fluxes. Notably, it does not rely on MCF emission estimates, which
 175 are highly uncertain after 2000 (McCulloch & Midgley, 2001).



176

177 **Figure 1.** Validation of ECCO-simulated tracer distributions against observations. Panels **a** and **b** show
 178 vertical sections of CFC-11 and MCF concentrations along the A16N2003 cruise track. Observations are
 179 shown as colored dots and the cruise path is indicated by the red line in the map inset in panel **a**. ECCO
 180 July monthly mean concentrations in 2003 are shown as colored shading, averaged longitudinally from
 181 20° W to 29° W. Data below 2.5 km are omitted in **a,b** due to near-zero concentrations. Tracer-tracer
 182 scatter plots of observed and modeled CFC-11 versus MCF are shown in three depth ranges: above
 183 0.5 km (**c**), 0.5–1 km (**d**), and 1–6 km (**e**). Black dots represent observations; red dots show ECCO output
 184 sampled at the nearest horizontal grid point and vertically interpolated to the observed depth. The
 185 strong agreement between ECCO and observed values indicates that the model realistically captures
 186 ocean tracer uptake and distributions for both CFC-11 and MCF.

187 3 Results

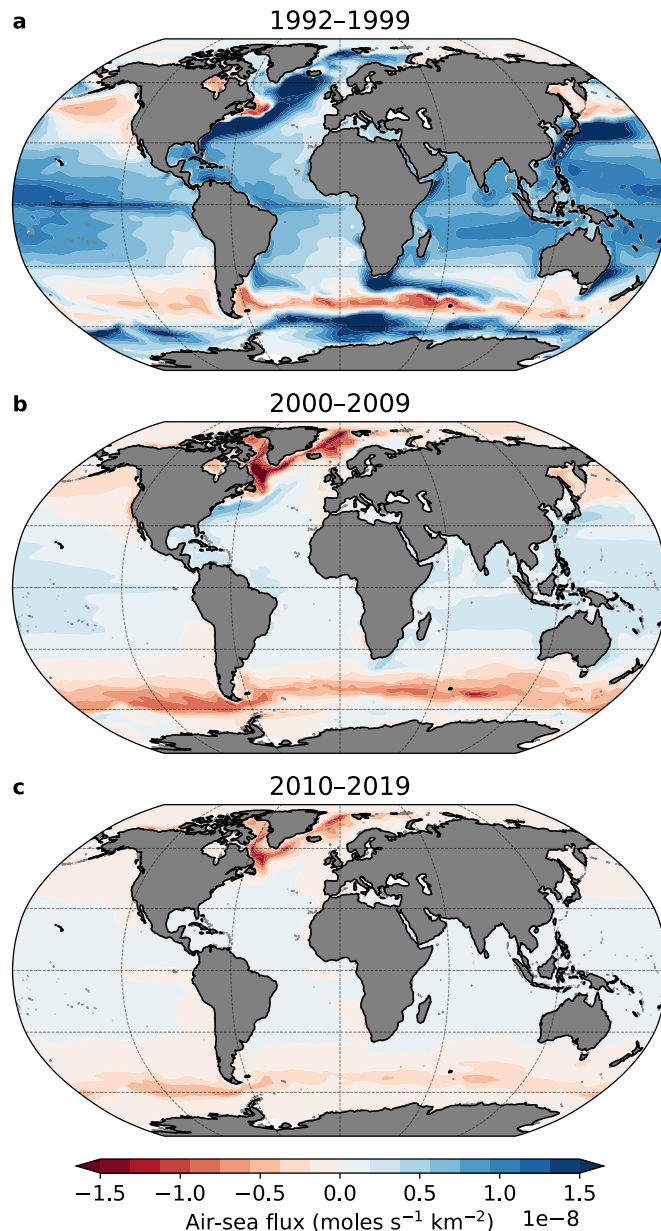
188 We first validate the ECCO simulation of ocean tracer uptake using CFC-11, which is a
 189 well-characterized and nearly conserved compound that has long served as a passive tracer for
 190 studying ocean circulation (e.g., Beismann & Redler, 2003; Bullister & Weiss, 1983; Dutay et al.,
 191 2002; England et al., 1994; Ito et al., 2004; Romanou et al., 2017; Wanninkhof, 1992, 2014;

192 Waugh, 2014). In this context, measured CFC-11, whose thermodynamic properties are well
193 known for estimating ocean physical uptake and was not used in the ECCO state estimation,
194 serves as independent evidence to test ECCO tracer uptake and distribution (Forget et al.,
195 2015b). Importantly, both MCF and CFC-11 were measured simultaneously along the A16N2003
196 cruise, enabling a consistent tracer-tracer comparison. Figure 1 presents both the absolute
197 concentrations and tracer-tracer scatter plots of CFC-11 and MCF from the ECCO simulation and
198 the A16N2003 observation. The model broadly captures the observed latitudinal and depth
199 distributions of both tracers, showing higher concentrations at high latitudes and in deeper
200 waters, where surface solubility is elevated (due to lower temperatures) and where deep-water
201 forms, facilitating tracer penetration.

202 The MCF results shown in Figure 1 represent our best estimate from the ECCO
203 simulation after updating two key parameters from W04: solubility and hydrolysis rate (see
204 Supplementary Text S1, S2 and Figure S4). Using the same freshwater solubility and hydrolysis
205 rate for MCF as in W04 would lead to an overestimation of ocean concentrations in the model
206 (Supplementary Figure S4 top row). However, updating the solubility based on a laboratory-
207 measured salting-out coefficient (Gossett, 1987), while keeping the hydrolysis rate unchanged,
208 shifts the modeled MCF concentrations toward the lower end of the observed range
209 (Supplementary Figure S4 middle row). However, we note that these hydrolysis losses of MCF
210 were primarily extracted from rates measured at temperatures between 25 °C and 120 °C
211 (Gerkens & Franklin, 1989), introducing substantial uncertainties in colder extratropical ocean
212 waters (Naus et al., 2021; Wennberg et al., 2004). We find better agreement between the
213 model and observations when the hydrolysis rate is reduced (i.e., slowed down), particularly at
214 colder temperatures. Note this adjusted hydrolysis rate remains well within the reported
215 uncertainty range (Gerkens & Franklin, 1989) (see Supplementary Figure S3).

216 Figure 2 shows ECCO-simulated spatial distributions of air-sea MCF fluxes over the past
217 three decades successively. In the 1990s, the global ocean acted predominantly as a sink for
218 MCF across most regions. Since the 2000s, however, the tropics have remained a sink while the
219 extratropical oceans are expected to have begun outgassing MCF. Intriguingly, this spatial flux
220 pattern is opposite to that of many other trace gases, such as CFC-11, HCFCs, HFCs, and CO₂,
221 which are typically taken up by the ocean at high latitudes and released to the atmosphere in
222 the tropics (DeVries et al., 2017; Gruber et al., 2009; Wang et al., 2021, 2023). This distinct
223 pattern for MCF is primarily driven by its strong temperature-dependent hydrolysis in the
224 ocean. Based on the hydrolysis parameters used in our simulation, MCF has a half-life on the
225 order of less than a year in warm tropical waters (~25 °C), but this extends to several decades in
226 extratropical oceans where sea surface temperature drops below 10 °C. As atmospheric MCF
227 concentrations have declined rapidly under the Montreal Protocol, the tropical ocean remains
228 undersaturated and continues to uptake MCF, due to rapid in situ degradation. In contrast, the

229 extratropics become oversaturated and outgas MCF because of much slower chemical loss in
 230 the surface ocean.

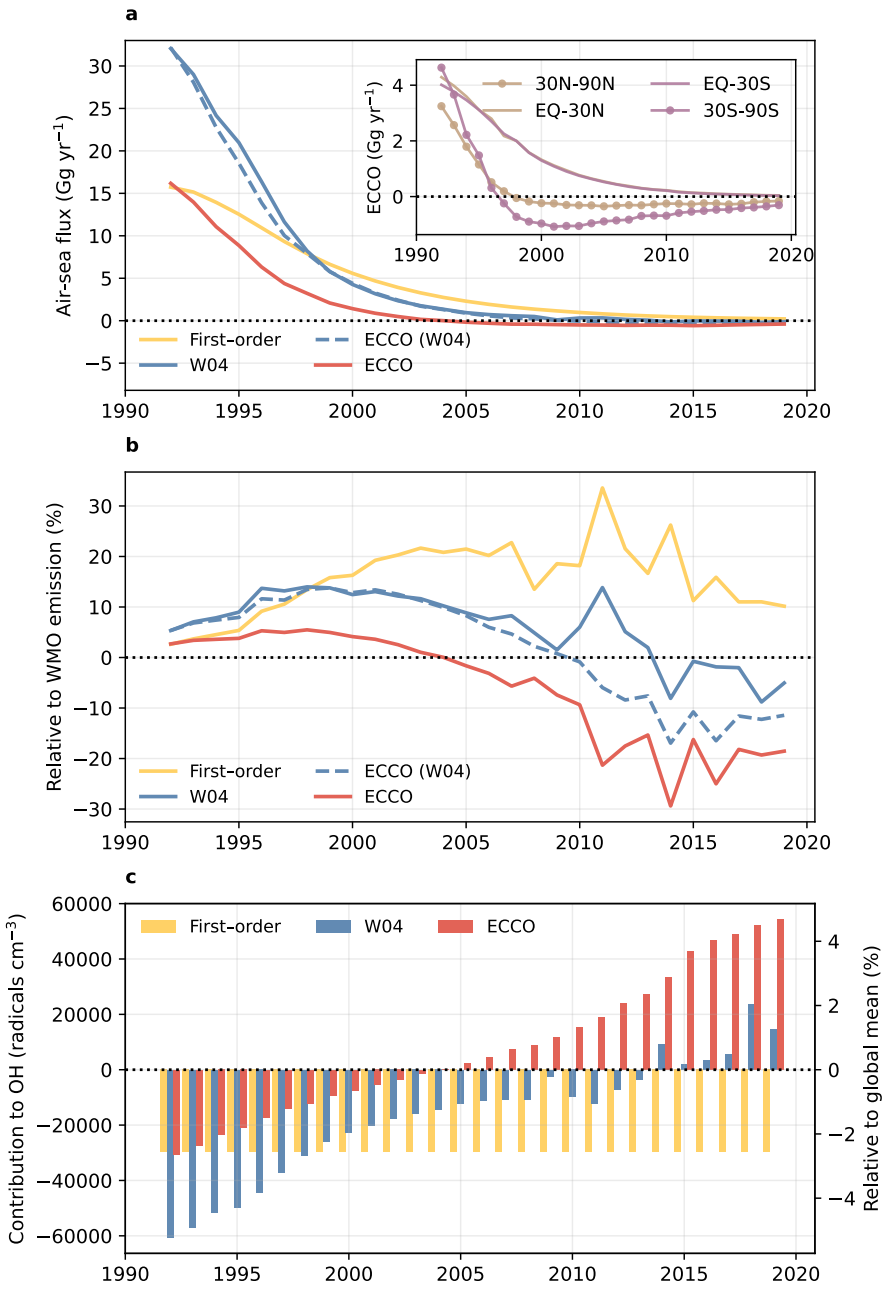


231

232 **Figure 2.** Spatial patterns of air-sea fluxes of MCF are shown as decadal averages for three time periods:
 233 1992–1999 (a), 2000–2009 (b), and 2010–2019 (c). Positive values (blue) indicate ocean uptake;
 234 negative values (red) indicate ocean outgassing.

235 To place our simulation in the context of earlier ocean representations, Figure 3a shows
 236 the globally integrated air-sea MCF flux for various ocean assumptions. Prior studies have often
 237 represented ocean uptake as a simple first-order loss process (e.g., assuming a constant oceanic
 238 partial lifetime of 197 years; Patra et al., 2011, 2014). Under this assumption, the oceanic loss in
 239 each year is calculated by simply dividing the atmospheric MCF burden by the oceanic partial

240 lifetime. This approach provides a reasonable approximation in the 1990s, when the global
 241 ocean acted as a net sink for MCF, and uptake was largely driven by high atmospheric MCF
 242 burden due to large anthropogenic emissions. However, as emissions declined rapidly after the
 243 1990s, the first-order loss assumption becomes increasingly inadequate, particularly in later
 244 years, because it assumes the ocean is always a net sink and does not account for the possibility
 245 of outgassing.



246

247 **Figure 3.** Time series of spatially integrated MCF air-sea fluxes and their impacts on inferred emissions
 248 and OH levels. Panel a shows comparison of global MCF air-sea fluxes from different ocean
 249 representations: first-order loss with an ocean partial lifetime of 197 years (yellow), an ocean general

250 circulation model used in W04 (blue), and ECCO simulations in this study. The ECCO run using the same
 251 freshwater solubility and hydrolysis rate as W04 is shown as the blue dashed line. The best estimate
 252 from ECCO — corrected for seawater solubility and with a slower cold-temperature hydrolysis rate — is
 253 shown as the red solid line. The inset panel in **a** shows the ECCO best estimate air-sea fluxes of MCF
 254 separately integrated over four latitude bands: 30° N–90° N, 30° N–equator, equator–30° S, and 30° S–
 255 90° S. Positive values indicate ocean uptake, and negative values indicate ocean outgassing. Panel **b**
 256 shows the same air-sea fluxes data in **a** but relative to top-down MCF emissions inferred in the WMO
 257 2022 Ozone Assessment report (Laube & Tegtmeier, 2022). Panel **c** shows the change in inferred OH
 258 that would be required to account for the air-sea MCF fluxes, if assuming the fluxes reflect changes in
 259 atmospheric MCF due to OH variations rather than atmosphere-ocean exchange (see Section 2.3 for
 260 details). The left y-axis indicates the absolute OH concentration (in radicals cm⁻³), and the right y-axis
 261 shows the corresponding relative change with respect to the global mean OH level of 1.16×10^6 radicals
 262 cm⁻³ (Spivakovsky et al., 2000).

263 The ECCO-simulated air-sea MCF flux, based on a time-varying ocean state, closely
 264 matches the W04 model, which uses a climatological ocean state, when the same freshwater
 265 solubility and hydrolysis rate parameters are applied (compare the blue solid and dashed lines
 266 in Figure 3**a**). This suggests that the oceanic MCF uptake is not strongly sensitive to the choice
 267 of ocean physical state. However, after accounting for seawater solubility and adopting a
 268 slower cold-temperature hydrolysis rate, the ocean acts as a significantly smaller reservoir for
 269 MCF — ocean uptake in the 1990s is reduced by more than 50%, and the onset of net
 270 outgassing occurs approximately five years in advance. This reduced ocean MCF uptake is
 271 driven primarily by the correction to seawater solubility, rather than adopting a slower
 272 hydrolysis rate, as demonstrated by additional sensitivity tests in Supplementary Figure S7.

273 Figure 3**b** compares the relative magnitude of various air-sea flux estimates to the top-
 274 down MCF emissions inferred in the World Meteorological Organization (WMO) 2022 Ozone
 275 Assessment report (Laube & Tegtmeier, 2022). In the 2010s, the inferred total MCF emissions
 276 were approximately 2.9 Gg yr⁻¹, even though reported consumption had dropped to zero (Rigby
 277 et al., 2017). While this estimated MCF emission relies on a climatological OH field (Rigby et al.,
 278 2013; Spivakovsky et al., 2000) — and the values may vary somewhat depending on the
 279 assumed OH levels — the ECCO simulation estimates suggest that the global ocean outgasses
 280 about 0.5 Gg yr⁻¹ of MCF back to the atmosphere, accounting for ~20% (and in some years up to
 281 30%) of the inferred total emissions during the same period. It is also important to note that
 282 the top-down estimates in Figure 3**b** are based on a first-order ocean loss with a partial lifetime
 283 of 94 years (Laube & Tegtmeier, 2022; Yvon-Lewis & Butler, 2002), which assumes the ocean
 284 continued to act as a net sink for MCF in the 2010s (at ~1.0 Gg yr⁻¹), despite the possibility that
 285 it had already become a net source. As a result, this inferred land-based MCF emission (Laube &
 286 Tegtmeier, 2022) can be largely overestimated (by up to 1.5 Gg yr⁻¹ in the 2010s).

287 Estimates of contributions to MCF-inferred OH due to different ocean representations
 288 are shown in Figure 3**c**. When the ocean acts as a net sink for MCF, accounting for air-sea fluxes
 289 lowers the inferred OH concentration because ocean uptake competes with OH as a sink for
 290 atmospheric MCF, reducing the amount of OH needed to balance the MCF mass budget. In
 291 contrast, when the ocean is a net source of MCF, including ocean outgassing increases the

292 inferred OH level, since more OH is required to remove the additional MCF released from the
293 ocean. To assess potential changes in inferred OH when using ECCO fluxes compared to earlier
294 ocean representations, if one assumes that the ocean uptakes more MCF or only weakly
295 outgasses MCF (e.g., W04 and first-order loss), but in reality the ocean uptakes less MCF before
296 2005 and outgasses more after 2005 (as simulated by ECCO), then the inferred OH levels would
297 be higher when using ECCO fluxes than when using W04 or first-order loss assumptions (by as
298 much as about 6% in recent years). Note that this estimated impact of switching ocean
299 representations on global mean OH assumes fixed emissions; part of the change in air-sea
300 fluxes could instead offset MCF emissions if emissions and OH were jointly optimized.

301 **4 Summary and Discussion**

302 We simulate MCF ocean uptake as accurately as current constraints allow — using an
303 ocean state estimate from ECCO and prescribed observed atmospheric MCF mole fractions. In
304 particular, by correcting for MCF seawater solubility as well as a slower cold-temperature
305 hydrolysis rate, our modeled ocean MCF concentrations show good agreement with depth-
306 resolved observations across a wide range of latitudes from a 2003 North Atlantic cruise. We
307 find that in the 2010s, ocean outgassing of MCF from ECCO ($\sim 0.5 \text{ Gg yr}^{-1}$) is substantially larger
308 than previous estimates, based either on simple first-order loss assumptions (which suggest
309 continued ocean uptake of up to $\sim 1 \text{ Gg yr}^{-1}$) or on a time-varying ocean flux from W04 (which
310 estimates outgassing at $\sim 0.03 \text{ Gg yr}^{-1}$). This is qualitatively consistent with a recent inversion
311 study (Naus et al., 2021), which suggested that a much larger high-latitude ocean source than
312 W04 is needed to explain the observed intra-hemispheric gradient in atmospheric MCF mole
313 fractions. Although the global ocean does not become a net source of MCF until after around
314 2005, the extratropical ocean appears to have begun outgassing as early as the late 1990s
315 (Figure 3a, insert panel). This raises the possibility that changes in atmospheric MCF mole
316 fractions previously attributed to European landfill emissions around the 2000s (Krol et al.,
317 2003; Reimann et al., 2005) may instead reflect contributions from the ocean, particularly given
318 that the subpolar North Atlantic emerges as a hot spot for ocean outgassing (Figure 2b,c).

319 As the observed decline in atmospheric MCF mole fractions slowed, previous inversion
320 models that relied on smaller ocean outgassing estimates compensated for this bias by
321 adjusting emissions to higher values, or invoking a decrease in atmospheric OH, or both, to
322 balance the MCF mass budget. In contrast, ECCO indicates a large ocean source of MCF,
323 potentially helping to explain the observed slowdown in the decay of atmospheric MCF mole
324 fractions without invoking a substantial OH decrease or persistent emissions. Most importantly,
325 our study suggests that the large MCF ocean source could account for as much as about 6% of
326 the 10–15% discrepancy between modelled and estimated absolute OH levels in recent years
327 (Naik et al., 2013; Prather et al., 2012; Prinn et al., 2005).

328 Future inversion studies — particularly with three-dimensional atmospheric models
329 (Naus et al., 2021; Patra et al., 2021) that incorporate spatially and temporally resolved MCF
330 air-sea fluxes from ECCO or other ocean reanalyses — could offer additional insights into the
331 spatiotemporal variability of OH. Such an approach would better disentangle oceanic and

anthropogenic MCF sources and provide estimates of absolute OH concentrations across latitudes. Notably, process-based chemistry-climate models tend to produce larger hemispheric OH ratios than those inferred from MCF-based inversions (Naik et al., 2013; Patra et al., 2014; Stevenson et al., 2020). Our results show that the Southern Hemisphere outgasses roughly twice as much MCF as the Northern Hemisphere, indicating that accounting for hemispheric asymmetries in ocean fluxes of MCF may substantially affect inferred interhemispheric OH distributions. Although estimates of Southern Ocean outgassing can carry large uncertainties due to both the challenges of modeling its complex ventilation (Dutay et al., 2002) and the paucity of direct oceanic MCF measurements in this region. Frequent low-pressure storms over the Southern Ocean can further complicate estimates by altering total barometric pressure and, in turn, influencing air-sea gas exchange (Kelly et al., 2025). Additionally, our study adjusted the MCF hydrolysis rate at cold temperatures beyond the range of existing laboratory measurements to improve agreement between the model and observations. Future work that directly measures MCF hydrolysis rates under ocean-relevant conditions would help reduce these uncertainties, particularly for high latitudes.

With the rapid decline in MCF emissions, which have become poorly constrained in recent decades, OH inversion studies are also exploring alternative tracers, such as HCFCs and HFCs (Liang et al., 2017), CO (Chen et al., 2025) and CO isotope (Krol et al., 2008; Morgenstern et al., 2025), formaldehyde (Wells et al., 2020; Wolfe et al., 2019), and methane (Penn et al., 2025). While promising, these substitutes face several limitations: shorter observational records than MCF, more complex source and sink processes beyond OH, and some methods offer only regional rather than global constraints on OH. Given these challenges, accurately characterizing OH levels inferred from MCF remains important, as it can provide a valuable benchmark for evaluating OH estimates derived from alternative tracers. Accounting for air-sea exchange of MCF is critical for improving the fidelity of OH inversions — especially in recent years, when ocean outgassing may constitute a substantial fraction of the total source and thus introduce biases in top-down estimates if this process is neglected or highly simplified.

359

360 Acknowledgments

361 P.W. gratefully acknowledges helpful discussions with Wei Chen, Qindan Zhu, and Gael Forget.
362 S.S. and P.W. acknowledge support from the National Science Foundation Atmospheric
363 Chemistry Division under grant 2128617. S.A.Y. acknowledges support from the CLIVAR repeat
364 hydrography program which is a joint effort between NOAA and NSF-OCE. M.R. received
365 funding from the UK Natural Environment Research Council Highlight Topic, InHALE
366 (Investigating HALocarbon impacts on the global Environment; NE/X00452X/1) and the NASA
367 Upper Atmosphere Research Program AGAGE grant 80NSSC21K1369. The computations
368 presented here were conducted using the “Svante” cluster, a facility located at MIT’s
369 Massachusetts Green High Performance Computing Center and supported by the Center for
370 Sustainability Science and Strategy (<https://cs3.mit.edu>).

371

372 **Open Research**

373 A16N2003 cruise data is available at <https://www.pmel.noaa.gov/co2/story/A16N>. AGAGE
374 atmospheric mole fractions data is available at <https://www-air.larc.nasa.gov/missions/agage/>.
375 Gridded ECCO monthly air-sea fluxes, ocean concentrations for CFC-11 and MCF, and code used
376 to generate all the figures in this analysis are available at Zenodo
377 (<https://doi.org/10.5281/zenodo.16648860>).
378

379 **References**

- 380 Beismann, J.-O., & Redler, R. (2003). Model simulations of CFC uptake in North Atlantic Deep
381 Water: Effects of parameterizations and grid resolution. *Journal of Geophysical*
382 *Research: Oceans*, 108(C5). <https://doi.org/10.1029/2001JC001253>
- 383 Bullister, J. L., & Weiss, R. F. (1983). Anthropogenic Chlorofluoromethanes in the Greenland and
384 Norwegian Seas. *Science*, 221(4607), 265–268.
385 <https://doi.org/10.1126/science.221.4607.265>
- 386 Bullister, John L., & Gruber, N. (2012). CRUISE REPORT: A16N_2003a [Data set].
387 https://cchdo.ucsd.edu/cruise/33RO200306_01
- 388 Burkholder, J. B., Sander, S. P., Abbatt, J., Barker J. R., Cappa, C., Crounse, J. D., Dibble, T. S.,
389 Huie, R. E., Kolb, C. E., Kurylo, M. J., Orkin, V. L., Percival, C. J., Wilmouth, D. M., and
390 Wine, P. H. Chemical Kinetics and Photochemical Data for Use in Atmospheric Studies,
391 Evaluation No. 19, JPL Publication 19-5, Jet Propulsion Laboratory, Pasadena, 2019
392 <http://jpldataeval.jpl.nasa.gov>.
- 393 Butler, J. H., Elkins, J. W., Thompson, T. M., Hall, B. D., Swanson, T. H., & Koropalov, V. (1991).
394 Oceanic consumption of CH₃CCl₃: Implications for tropospheric OH. *Journal of*
395 *Geophysical Research: Atmospheres*, 96(D12), 22347–22355.
396 <https://doi.org/10.1029/91JD02126>
- 397 Chen, W., Zhang, Y., & Liang, R. (2025). Converging evidence for reduced global atmospheric
398 oxidation in 2020. *National Science Review*, nwaf232.
399 <https://doi.org/10.1093/nsr/nwaf232>
- 400 DeVries, T., Holzer, M., & Primeau, F. (2017). Recent increase in oceanic carbon uptake driven
401 by weaker upper-ocean overturning. *Nature*, 542(7640), 215–218.
402 <https://doi.org/10.1038/nature21068>
- 403 Dutay, J.-C., Bullister, J. L., Doney, S. C., Orr, J. C., Najjar, R., Caldeira, K., et al. (2002). Evaluation
404 of ocean model ventilation with CFC-11: comparison of 13 global ocean models. *Ocean*
405 *Modelling*, 4(2), 89–120.
- 406 England, M. H., Garçon, V., & Minster, J.-F. (1994). Chlorofluorocarbon uptake in a world ocean
407 model: 1. Sensitivity to the surface gas forcing. *Journal of Geophysical Research: Oceans*,
408 99(C12), 25215–25233. <https://doi.org/10.1029/94JC02205>

- 409 Forget, G., Campin, J.-M., Heimbach, P., Hill, C. N., Ponte, R. M., & Wunsch, C. (2015a). ECCO
410 version 4: an integrated framework for non-linear inverse modeling and global ocean
411 state estimation. *Geoscientific Model Development*, 8(10), 3071–3104.
412 <https://doi.org/10.5194/gmd-8-3071-2015>
- 413 Forget, G., Ferreira, D., & Liang, X. (2015b). On the observability of turbulent transport rates by
414 Argo: supporting evidence from an inversion experiment. *Ocean Science*, 11(5), 839–
415 853. <https://doi.org/10.5194/os-11-839-2015>
- 416 Gerkens, R. R., & Franklin, J. A. (1989). The rate of degradation of 1,1,1-trichloroethane in water
417 by hydrolysis and dehydrochlorination. *Chemosphere*, 19(12), 1929–1937.
418 [https://doi.org/10.1016/0045-6535\(89\)90016-7](https://doi.org/10.1016/0045-6535(89)90016-7)
- 419 Gossett, J. M. (1987). Measurement of Henry's law constants for C1 and C2 chlorinated
420 hydrocarbons. *Environmental Science & Technology*, 21(2), 202–208.
421 <https://doi.org/10.1021/es00156a012>
- 422 Gruber, N., Gloor, M., Mikaloff Fletcher, S. E., Doney, S. C., Dutkiewicz, S., Follows, M. J., et al.
423 (2009). Oceanic sources, sinks, and transport of atmospheric CO₂. *Global
424 Biogeochemical Cycles*, 23(1). <https://doi.org/10.1029/2008GB003349>
- 425 Ito, T., Marshall, J., & Follows, M. (2004). What controls the uptake of transient tracers in the
426 Southern Ocean? *Global Biogeochemical Cycles*, 18(2).
- 427 Kelly, C. L., Chang, B. X., Emmanuelli, A. F., Park, E. R., Macdonald, A. M., & Nicholson, D. P.
428 (2025, April 30). Low-pressure storms drive nitrous oxide emissions in the Southern
429 Ocean. Research Square. <https://doi.org/10.21203/rs.3.rs-6378208/v1>
- 430 Krol, M., & Lelieveld, J. (2003). Can the variability in tropospheric OH be deduced from
431 measurements of 1,1,1-trichloroethane (methyl chloroform)? *Journal of Geophysical
432 Research: Atmospheres*, 108(D3). <https://doi.org/10.1029/2002JD002423>
- 433 Krol, M. C., Lelieveld, J., Oram, D. E., Sturrock, G. A., Penkett, S. A., Brenninkmeijer, C. A. M., et
434 al. (2003). Continuing emissions of methyl chloroform from Europe. *Nature*, 421(6919),
435 131–135. <https://doi.org/10.1038/nature01311>
- 436 Krol, M. C., Meirink, J. F., Bergamaschi, P., Mak, J. E., Lowe, D., Jöckel, P., et al. (2008). What can
437 ¹⁴CO measurements tell us about OH? *Atmospheric Chemistry and Physics*, 8(16), 5033–
438 5044. <https://doi.org/10.5194/acp-8-5033-2008>
- 439 Laube, J. C., & Tegtmeier, S. (2022). *Scientific Assessment of Ozone Depletion: 2022. Chapter 1:
440 Update on Ozone-Depleting Substances (ODSs) and Other Gases of Interest to the
441 Montreal Protocol* (No. 278) (p. 509). Geneva, Switzerland: World Meteorological
442 Organization.
- 443 Levy, H. (1971). Normal Atmosphere: Large Radical and Formaldehyde Concentrations
444 Predicted. *Science*, 173(3992), 141–143. <https://doi.org/10.1126/science.173.3992.141>
- 445 Liang, Q., Chipperfield, M. P., Fleming, E. L., Abraham, N. L., Braesicke, P., Burkholder, J. B., et al.
446 (2017). Deriving Global OH Abundance and Atmospheric Lifetimes for Long-Lived Gases:

- 447 A Search for CH₃CCl₃ Alternatives. *Journal of Geophysical Research: Atmospheres*,
448 122(21), 11,914–11,933. <https://doi.org/10.1002/2017JD026926>
- 449 Marshall, J., Adcroft, A., Hill, C., Perelman, L., & Heisey, C. (1997a). A finite-volume,
450 incompressible Navier Stokes model for studies of the ocean on parallel computers.
451 *Journal of Geophysical Research: Oceans*, 102(C3), 5753–5766.
- 452 Marshall, J., Hill, C., Perelman, L., & Adcroft, A. (1997b). Hydrostatic, quasi-hydrostatic, and
453 nonhydrostatic ocean modeling. *Journal of Geophysical Research: Oceans*, 102(C3),
454 5733–5752.
- 455 McCulloch, A., & Midgley, P. M. (2001). The history of methyl chloroform emissions: 1951–
456 2000. *Atmospheric Environment*, 35(31), 5311–5319. <https://doi.org/10.1016/S1352->
457 2310(01)00306-5
- 458 McNorton, J., Chipperfield, M. P., Gloor, M., Wilson, C., Feng, W., Hayman, G. D., et al. (2016).
459 Role of OH variability in the stalling of the global atmospheric CH₄ growth rate from
460 1999 to 2006. *Atmospheric Chemistry and Physics*, 16(12), 7943–7956.
461 <https://doi.org/10.5194/acp-16-7943-2016>
- 462 Montzka, S. A., Krol, M., Dlugokencky, E., Hall, B., Jöckel, P., & Lelieveld, J. (2011). Small
463 Interannual Variability of Global Atmospheric Hydroxyl. *Science*, 331(6013), 67–69.
464 <https://doi.org/10.1126/science.1197640>
- 465 Morgenstern, O., Moss, R., Manning, M., Zeng, G., Schaefer, H., Usoskin, I., et al. (2025).
466 Radiocarbon monoxide indicates increasing atmospheric oxidizing capacity. *Nature*
467 *Communications*, 16(1), 249. <https://doi.org/10.1038/s41467-024-55603-1>
- 468 Murray, L. T., Fiore, A. M., Shindell, D. T., Naik, V., & Horowitz, L. W. (2021). Large uncertainties
469 in global hydroxyl projections tied to fate of reactive nitrogen and carbon. *Proceedings*
470 *of the National Academy of Sciences*, 118(43), e2115204118.
471 <https://doi.org/10.1073/pnas.2115204118>
- 472 Naik, V., Voulgarakis, A., Fiore, A. M., Horowitz, L. W., Lamarque, J.-F., Lin, M., et al. (2013).
473 Preindustrial to present-day changes in tropospheric hydroxyl radical and methane
474 lifetime from the Atmospheric Chemistry and Climate Model Intercomparison Project
475 (ACCMIP). *Atmospheric Chemistry and Physics*, 13(10), 5277–5298.
476 <https://doi.org/10.5194/acp-13-5277-2013>
- 477 Naus, S., Montzka, S. A., Pandey, S., Basu, S., Dlugokencky, E. J., & Krol, M. (2019). Constraints
478 and biases in a tropospheric two-box model of OH. *Atmospheric Chemistry and Physics*,
479 19(1), 407–424. <https://doi.org/10.5194/acp-19-407-2019>
- 480 Naus, S., Montzka, S. A., Patra, P. K., & Krol, M. C. (2021). A three-dimensional-model inversion
481 of methyl chloroform to constrain the atmospheric oxidative capacity. *Atmospheric*
482 *Chemistry and Physics*, 21(6), 4809–4824. <https://doi.org/10.5194/acp-21-4809-2021>
- 483 Nicely, J. M., Duncan, B. N., Hanisco, T. F., Wolfe, G. M., Salawitch, R. J., Deushi, M., et al.
484 (2020). A machine learning examination of hydroxyl radical differences among model

- 485 simulations for CCM1-1. *Atmospheric Chemistry and Physics*, 20(3), 1341–1361.
486 <https://doi.org/10.5194/acp-20-1341-2020>
- 487 Patra, P. K., Houweling, S., Krol, M., Bousquet, P., Belikov, D., Bergmann, D., et al. (2011).
488 TransCom model simulations of CH₄ and related species: linking transport, surface flux
489 and chemical loss with CH₄ variability in the troposphere and lower stratosphere.
490 *Atmospheric Chemistry and Physics*, 11(24), 12813–12837. <https://doi.org/10.5194/acp-11-12813-2011>
- 492 Patra, P. K., Krol, M. C., Montzka, S. A., Arnold, T., Atlas, E. L., Lintner, B. R., et al. (2014).
493 Observational evidence for interhemispheric hydroxyl-radical parity. *Nature*, 513(7517),
494 219–223. <https://doi.org/10.1038/nature13721>
- 495 Patra, P. K., Krol, M. C., Prinn, R. G., Takigawa, M., Mühle, J., Montzka, S. A., et al. (2021).
496 Methyl Chloroform Continues to Constrain the Hydroxyl (OH) Variability in the
497 Troposphere. *Journal of Geophysical Research: Atmospheres*, 126(4), e2020JD033862.
498 <https://doi.org/10.1029/2020JD033862>
- 499 Penn, E., Jacob, D. J., Chen, Z., East, J. D., Sulprizio, M. P., Bruhwiler, L., et al. (2025). What can
500 we learn about tropospheric OH from satellite observations of methane? *Atmospheric
501 Chemistry and Physics*, 25(5), 2947–2965. <https://doi.org/10.5194/acp-25-2947-2025>
- 502 Prather, M., & Spivakovsky, C. M. (1990). Tropospheric OH and the lifetimes of
503 hydrochlorofluorocarbons. *Journal of Geophysical Research: Atmospheres*, 95(D11),
504 18723–18729. <https://doi.org/10.1029/JD095iD11p18723>
- 505 Prather, M. J., Holmes, C. D., & Hsu, J. (2012). Reactive greenhouse gas scenarios: Systematic
506 exploration of uncertainties and the role of atmospheric chemistry. *Geophysical
507 Research Letters*, 39(9). <https://doi.org/10.1029/2012GL051440>
- 508 Prinn, R., Cunnold, D., Simmonds, P., Alyea, F., Boldi, R., Crawford, A., et al. (1992). Global
509 average concentration and trend for hydroxyl radicals deduced from ALE/GAGE
510 trichloroethane (methyl chloroform) data for 1978–1990. *Journal of Geophysical
511 Research: Atmospheres*, 97(D2), 2445–2461. <https://doi.org/10.1029/91JD02755>
- 512 Prinn, R. G., Huang, J., Weiss, R. F., Cunnold, D. M., Fraser, P. J., Simmonds, P. G., et al. (2005).
513 Evidence for variability of atmospheric hydroxyl radicals over the past quarter century.
514 *Geophysical Research Letters*, 32(7). <https://doi.org/10.1029/2004GL022228>
- 515 Prinn, Ronald G, Weiss, R. F., Arduini, J., Arnold, T., DeWitt, H. L., Fraser, P. J., et al. (2018).
516 History of chemically and radiatively important atmospheric gases from the Advanced
517 Global Atmospheric Gases Experiment (AGAGE). *Earth System Science Data*, 10(2), 985–
518 1018.
- 519 Reimann, S., Manning, A. J., Simmonds, P. G., Cunnold, D. M., Wang, R. H. J., Li, J., et al. (2005).
520 Low European methyl chloroform emissions inferred from long-term atmospheric
521 measurements. *Nature*, 433(7025), 506–508. <https://doi.org/10.1038/nature03220>
- 522 Rigby, M., Prinn, R. G., O'Doherty, S., Montzka, S. A., McCulloch, A., Harth, C. M., et al. (2013).
523 Re-evaluation of the lifetimes of the major CFCs and CH₃CCl₃ using atmospheric trends.

- 524 *Atmospheric Chemistry and Physics*, 13(5), 2691–2702. <https://doi.org/10.5194/acp-13-2691-2013>
- 525
- 526 Rigby, Matthew, Montzka, S. A., Prinn, R. G., White, J. W. C., Young, D., O'Doherty, S., et al.
527 (2017). Role of atmospheric oxidation in recent methane growth. *Proceedings of the
528 National Academy of Sciences*, 114(21), 5373–5377.
529 <https://doi.org/10.1073/pnas.1616426114>
- 530 Romanou, A., Marshall, J., Kelley, M., & Scott, J. (2017). Role of the ocean's AMOC in setting the
531 uptake efficiency of transient tracers. *Geophysical Research Letters*, 44(11), 5590–5598.
- 532 Singh, H. B., Kanakidou, M., Crutzen, P. J., & Jacob, D. J. (1995). High concentrations and
533 photochemical fate of oxygenated hydrocarbons in the global troposphere. *Nature*,
534 378(6552), 50–54. <https://doi.org/10.1038/378050a0>
- 535 Spivakovsky, C. M., Logan, J. A., Montzka, S. A., Balkanski, Y. J., Foreman-Fowler, M., Jones, D. B.
536 A., et al. (2000). Three-dimensional climatological distribution of tropospheric OH:
537 Update and evaluation. *Journal of Geophysical Research: Atmospheres*, 105(D7), 8931–
538 8980. <https://doi.org/10.1029/1999JD901006>
- 539 Stevenson, D. S., Zhao, A., Naik, V., O'Connor, F. M., Tilmes, S., Zeng, G., et al. (2020). Trends in
540 global tropospheric hydroxyl radical and methane lifetime since 1850 from
541 AerChemMIP. *Atmospheric Chemistry and Physics*, 20(21), 12905–12920.
542 <https://doi.org/10.5194/acp-20-12905-2020>
- 543 Turner, A. J., Frankenberg, C., Wennberg, P. O., & Jacob, D. J. (2017). Ambiguity in the causes
544 for decadal trends in atmospheric methane and hydroxyl. *Proceedings of the National
545 Academy of Sciences*, 114(21), 5367–5372. <https://doi.org/10.1073/pnas.1616020114>
- 546 Wang, P., Scott, J. R., Solomon, S., Marshall, J., Babbin, A. R., Lickley, M., et al. (2021). On the
547 effects of the ocean on atmospheric CFC-11 lifetimes and emissions. *Proceedings of the
548 National Academy of Sciences*, 118(12), e2021528118.
549 <https://doi.org/10.1073/pnas.2021528118>
- 550 Wang, P., Solomon, S., Lickley, M., Scott, J. R., Weiss, R. F., & Prinn, R. G. (2023). On the
551 Influence of Hydroxyl Radical Changes and Ocean Sinks on Estimated HCFC and HFC
552 Emissions and Banks. *Geophysical Research Letters*, 50(18), e2023GL105472.
553 <https://doi.org/10.1029/2023GL105472>
- 554 Wanninkhof, R. (1992). Relationship between wind speed and gas exchange over the ocean.
555 *Journal of Geophysical Research: Oceans*, 97(C5), 7373–7382.
556 <https://doi.org/10.1029/92JC00188>
- 557 Wanninkhof, R. (2014). Relationship between wind speed and gas exchange over the ocean
558 revisited. *Limnology and Oceanography: Methods*, 12(6), 351–362.
559 <https://doi.org/10.4319/lom.2014.12.351>
- 560 Waugh, D. W. (2014). Changes in the ventilation of the southern oceans. *Philosophical
561 Transactions of the Royal Society A: Mathematical, Physical and Engineering Sciences*,
562 372(2019), 20130269. <https://doi.org/10.1098/rsta.2013.0269>

- 563 Wells, K. C., Millet, D. B., Payne, V. H., Deventer, M. J., Bates, K. H., de Gouw, J. A., et al. (2020).
564 Satellite isoprene retrievals constrain emissions and atmospheric oxidation. *Nature*,
565 585(7824), 225–233. <https://doi.org/10.1038/s41586-020-2664-3>
- 566 Wennberg, P. O., Peacock, S., Randerson, J. T., & Bleck, R. (2004). Recent changes in the air-sea
567 gas exchange of methyl chloroform. *Geophysical Research Letters*, 31(16).
568 <https://doi.org/10.1029/2004GL020476>
- 569 Wolfe, G. M., Nicely, J. M., St. Clair, J. M., Hanisco, T. F., Liao, J., Oman, L. D., et al. (2019).
570 Mapping hydroxyl variability throughout the global remote troposphere via synthesis of
571 airborne and satellite formaldehyde observations. *Proceedings of the National Academy
572 of Sciences*, 116(23), 11171–11180. <https://doi.org/10.1073/pnas.1821661116>
- 573 Yvon-Lewis, S. A., & Butler, J. H. (2002). Effect of oceanic uptake on atmospheric lifetimes of
574 selected trace gases. *Journal of Geophysical Research: Atmospheres*, 107(D20), ACH 1-1-
575 ACH 1-9. <https://doi.org/10.1029/2001JD001267>
- 576 Yvon-Lewis, S. A., King, D. B., Tokarczyk, R., Goodwin, K. D., Saltzman, E. S., & Butler, J. H.
577 (2004). Methyl bromide and methyl chloride in the Southern Ocean. *Journal of
578 Geophysical Research: Oceans*, 109(C2). <https://doi.org/10.1029/2003JC001809>
- 579 Zhu, Q., Fiore, A. M., Correa, G., Lamarque, J.-F., & Worden, H. (2024). The impact of internal
580 climate variability on OH trends between 2005 and 2014. *Environmental Research
581 Letters*, 19(6), 064032. <https://doi.org/10.1088/1748-9326/ad4b47>
- 582

1 **Ocean Outgassing of Methyl Chloroform as an Underestimated Source of Emission**

2

3 **Peidong Wang^{1*}, Susan Solomon¹, Jeffery R. Scott¹, Shari A. Yvon-Lewis², Paul O. Wennberg³,**
4 **Ray F. Weiss⁴, Matthew Rigby^{5,6}, Minde An⁶**

5

6 ¹Department of Earth, Atmospheric and Planetary Sciences, Massachusetts Institute of
7 Technology, Cambridge, MA, USA.

8 ²Department of Oceanography, Texas A&M University, College Station, TX, USA.

9 ³Division of Geological and Planetary Sciences, California Institute of Technology, Pasadena, CA,
10 USA.

11 ⁴Scripps Institution of Oceanography, University of California San Diego, La Jolla, CA, USA.

12 ⁵School of Chemistry, University of Bristol, Bristol, UK.

13 ⁶Center for Sustainability Science and Strategy, Massachusetts Institute of Technology,
14 Cambridge, MA, USA.

15

16 Corresponding author: Peidong Wang (pdwang@mit.edu)

17 **Key Points:**

- 18 • The ocean uptakes methyl chloroform (MCF) in the tropics and outgasses in the
19 extratropics, the reverse of many other tracers such as CFC-11
- 20 • Our model estimates that the ocean outgassed 0.5 Gg yr⁻¹ of MCF in the 2010s,
21 accounting for up to 30% of top-down inferred emissions
- 22 • This ocean outgassing is substantially larger than previous estimates and can
23 significantly affect inferred MCF emissions and OH levels

24

25 Abstract

26 Methyl chloroform (MCF) is a synthetic ozone-depleting substance used as an industrial solvent.
27 Its primary sink is reaction with the hydroxyl radical (OH), making it a key tracer for estimating
28 atmospheric oxidative capacity. Following Montreal Protocol regulations, MCF emissions
29 declined rapidly after the 1990s. However, the recent slowdown in atmospheric MCF decay
30 suggests persistent emissions and/or declining OH (contradicting chemistry-climate models
31 projecting increasing OH). The air-sea exchange of MCF has been poorly constrained due to
32 limited observations and simplified ocean representations. We simulate oceanic MCF fluxes
33 using a modern ocean reanalysis and validate with depth-resolved observations. Results
34 suggest the ocean has shifted from a net sink to a net source around 2005, outgassing 0.5 Gg yr^{-1}
35 in the 2010s (up to 30% of inferred MCF emissions). This ocean outgas is an order of
36 magnitude larger than previous estimates and can have important implications for interpreting
37 OH levels from MCF records.

38

39 Plain Language Summary

40 Methyl chloroform (MCF) is a human-made compound that depletes stratospheric ozone, and
41 its production has been phased out under the Montreal Protocol. However, recent observations
42 show that atmospheric MCF is declining more slowly than expected, suggesting the presence of
43 unexplained emissions and/or a decrease in hydroxyl radical (OH) levels (at odds with
44 chemistry-climate models that suggest OH should have remained stable or increased). As
45 anthropogenic MCF emissions have declined, the role of the ocean in both uptake and
46 outgassing of MCF has grown more significant, but this component has been largely overlooked
47 in previous studies. Here, we simulate ocean uptake and outgassing of MCF as accurately as
48 current constraints allow. We find that the global ocean likely shifted to a net source of
49 emission around 2005, releasing MCF at levels substantially higher than previously thought.
50 Global OH levels are typically inferred from measurements of atmospheric MCF, which is
51 primarily removed through reactions with OH, so changes in the MCF source strength in turn
52 imply changes in atmospheric OH, which may be as large as ~6% in the past few years. These
53 results highlight the importance of accurately representing air-sea exchange in atmospheric
54 trace gas budgets and inferences of OH levels.

55

56 1 Introduction

57 The hydroxyl radical (OH) is the primary atmospheric oxidant (Levy, 1971). OH governs
58 the lifetimes of key greenhouse gases including methane (McNorton et al., 2016; Prather et al.,
59 2012; Prather & Spivakovsky, 1990; Rigby et al., 2017; Turner et al., 2017) and various
60 halocarbons (Liang et al., 2017; Prather & Spivakovsky, 1990; Rigby et al., 2013) (e.g.,
61 hydrochlorofluorocarbons [HCFCs] and hydrofluorocarbons [HFCs]), and it also influences air
62 pollution through its role in tropospheric ozone chemistry (Levy, 1971; Singh et al., 1995).
63 Therefore, accurately characterizing atmospheric OH is crucial for estimating greenhouse gas
64 emissions as well as informing air pollution mitigation efforts. However, due to its extremely

65 short atmospheric lifetime of about one second, OH cannot be directly measured on a global
66 scale. Instead, global mean OH concentrations are most commonly inferred indirectly, from
67 observations of atmospheric methyl chloroform (CH_3CCl_3 ; MCF) (e.g., Krol & Lelieveld, 2003;
68 Montzka et al., 2011; Naus et al., 2019; Patra et al., 2014; Prather et al., 2012; Prinn et al., 1992;
69 Spivakovsky et al., 2000) — a relatively long-lived synthetic compound that has been globally
70 monitored since 1978 (Prinn et al., 2018) and is predominantly removed by reaction with OH.

71 However, critical yet unresolved discrepancies remain between OH levels inferred from
72 MCF using inverse modeling approaches and those simulated directly by process-based
73 chemistry-climate models based on known OH chemistry. Process-based chemistry-climate
74 models tend to overestimate absolute OH levels inferred from MCF by 10–15% (Naik et al.,
75 2013; Prather et al., 2012; Prinn et al., 2005). Chemistry-climate models also suggest stable or
76 slightly increasing OH (Stevenson et al., 2020; Zhu et al., 2024), which conflicts with some MCF
77 inverse modeling studies indicating a post-2005 decline (Rigby et al., 2017; Turner et al., 2017).
78 Although process-based OH levels show substantial spread across models (Murray et al., 2021;
79 Naik et al., 2013), MCF-based estimates can also carry large uncertainties and show differences
80 between studies, raising concerns about their continued reliability for the inference of global
81 OH (Nicely et al., 2020; Patra et al., 2021).

82 Inferring OH from MCF relies on knowledge of its source and sink terms. MCF is a
83 stratospheric ozone-depleting substance and its anthropogenic emissions have declined rapidly
84 due to controls of the Montreal Protocol (Laube & Tegtmeier, 2022). While bottom-up
85 inventories provide well-constrained MCF production and emission estimates prior to 2000
86 (McCulloch & Midgley, 2001), they have been poorly characterized in the years since. To
87 address this issue in quantifying OH, recent studies seek to simultaneously optimize both
88 anthropogenic MCF emissions and OH concentrations in joint inversions (e.g., Naus et al., 2021;
89 Rigby et al., 2017; Turner et al., 2017). However, other potential natural source and sink terms
90 for MCF (i.e., from ocean uptake and outgassing) are proportionally increasing their significance
91 as anthropogenic emissions have declined, introducing biases if these processes are poorly
92 represented or overlooked in the inversion. Studies have suggested unexplained emissions
93 occurring at least since 2013 (Naus et al., 2021; Rigby et al., 2017; Turner et al., 2017), when
94 global MCF consumption should have ceased (Rigby et al., 2017). A recent three-dimensional
95 model inversion further attributes these unexplained emissions primarily to high latitudes, and
96 suggested that the ocean could be a missing source (Naus et al., 2021).

97 Oceanic uptake and outgassing of MCF have been rather ambiguously represented in
98 previous OH inversions. MCF can dissolve in seawater and undergo further degradation through
99 hydrolysis (Butler et al., 1991; Gerkens & Franklin, 1989; Yvon-Lewis & Butler, 2002). Earlier
100 studies either neglect this process altogether or treat the ocean as a simple first-order loss term
101 (Patra et al., 2011, 2014; Prather et al., 2012; Turner et al., 2017). A more complex, time-
102 varying ocean uptake of MCF using an ocean general circulation model (Wennberg et al., 2004;
103 hereafter W04) has only been incorporated in OH inversion studies recently (Patra et al., 2021;
104 Rigby et al., 2017), and this oceanic term has been shown to be a dominant sensitivity factor for
105 inferred OH (Rigby et al., 2017). However, W04 extends their projections of MCF air-sea fluxes

106 beyond the 2000s, when atmospheric MCF observations were not available to constrain their
107 model. Moreover, W04 uses the freshwater solubility of MCF, which may overestimate
108 seawater uptake. Combined with limited ocean observations, their air-sea flux remains highly
109 uncertain (Naus et al., 2021; Wennberg et al., 2004) and appears insufficient to account for the
110 high-latitude source inferred in recent inversions (Naus et al., 2021; Rigby et al., 2017).

111 In this study, we simulate the ocean uptake and outgassing of MCF from 1992 to 2019
112 using the Estimating the Circulation and Climate of the Ocean (ECCO) framework (Forget et al.,
113 2015a), which provides a physically consistent, observationally-constrained reconstruction of
114 the global ocean. And by prescribing observed MCF atmospheric mole fractions from the
115 Advanced Global Atmospheric Gases Experiment (AGAGE) network (Prinn et al., 2018), the
116 model enables a realistic simulation of the oceanic uptake of MCF. A key strength of our study
117 is the validation of simulated MCF distributions using an extensive set of depth-resolved ocean
118 profile observations from a North Atlantic cruise conducted in July 2003 (A16N2003). We then
119 evaluate the magnitude of ECCO-simulated MCF ocean outgassing relative to inferred total
120 emissions, compare it with previous estimates, and discuss its potential implications for
121 inferred OH abundances.

122 **2 Materials and Methods**

123 2.1 Sampling during the A16N2003 cruise

124 Depth-resolved observations of CFC-11 and MCF were collected during the A16N2003
125 cruise aboard the National Oceanic and Atmospheric Administration (NOAA) R/V *Ronald H.*
126 *Brown*, during June to August in 2003. Nearly all simultaneous measurements of CFC-11 and
127 MCF were taken in July, spanning 44 stations from 45.5° N to 2° S along longitudes 20° W to
128 29° W. The cruise track is shown in Figure 1a insert panel with the red line. During this cruise,
129 over 600 data points were collected for each tracer, with maximum depth at ~5,900 m. Detailed
130 descriptions of the measurement and sampling techniques are provided in (Bullister & Gruber,
131 2012; Yvon-Lewis et al., 2004).

132 2.2 Ocean state estimate and atmospheric forcing

133 The ocean state is represented by ECCO Version 4 Release 5 (Forget et al., 2015a), which
134 assimilates satellite and in situ observations using the Massachusetts Institute of Technology
135 General Circulation Model (MITgcm; Marshall et al., 1997a, 1997b) to produce a physically
136 consistent ocean reanalysis from 1992 to 2019. The ECCO simulation is run on the Lat-Lon-Cap
137 90 (LLC90) grid, with a horizontal resolution of approximately 1°, 50 vertical layers extending to
138 ~6,100 m depth, and a time step of one hour. Modeled tracer concentrations and air-sea fluxes
139 outputs are archived as monthly means, gridded on a regular 1° × 1° horizontal grid from the
140 LLC90 grid.

141 We couple the ECCO ocean with monthly values of atmospheric mole fractions of CFC-
142 11 and MCF from the AGAGE 12-box model output (Rigby et al., 2013). This 12-box model uses
143 prior emission estimates for CFC-11 and MCF before 1978, and posterior emissions constrained

144 by AGAGE observations thereafter. As a result, it provides continuous monthly mole fractions
 145 for both species starting from a time when their atmospheric concentrations were effectively
 146 zero, allowing ocean accumulation to begin, and closely matches observations after 1978 (see
 147 Supplementary Figures S1 and S2 for CFC-11 and MCF, respectively). The lower tropospheric
 148 mole fractions are provided across four latitude bands: 30° N–90° N, 30° N–equator, equator–
 149 30° S, and 30° S–90° S. To estimate spatially continuous air-sea fluxes, we linearly interpolate
 150 the atmospheric mole fractions every 10° of latitude across the boundaries of adjacent latitude
 151 bands (i.e., linearly interpolate from 35° N to 25° N, 5° N to 5° S, and 25° S to 35° S).

152 Because ECCO simulates time-varying ocean states that closely reflect observations only
 153 after 1992, we use the 1992 ocean state as a fixed boundary condition to estimate the initial
 154 distributions of CFC-11 and MCF. Specifically, we repeat the 1992 forcing fields in ECCO while
 155 prescribing time-varying atmospheric mole fractions starting from 1951 for both CFC-11 and
 156 MCF, allowing for tracer uptake and accumulation over time. This approach yields a reasonable
 157 estimate of the initial tracer distribution in the ocean by 1992. All results presented in this study
 158 focus on the period from 1992 onward.

159 Detailed descriptions of MCF solubility and hydrolysis, as well as air-sea exchange
 160 parameterizations, are provided in the Supplementary Text.

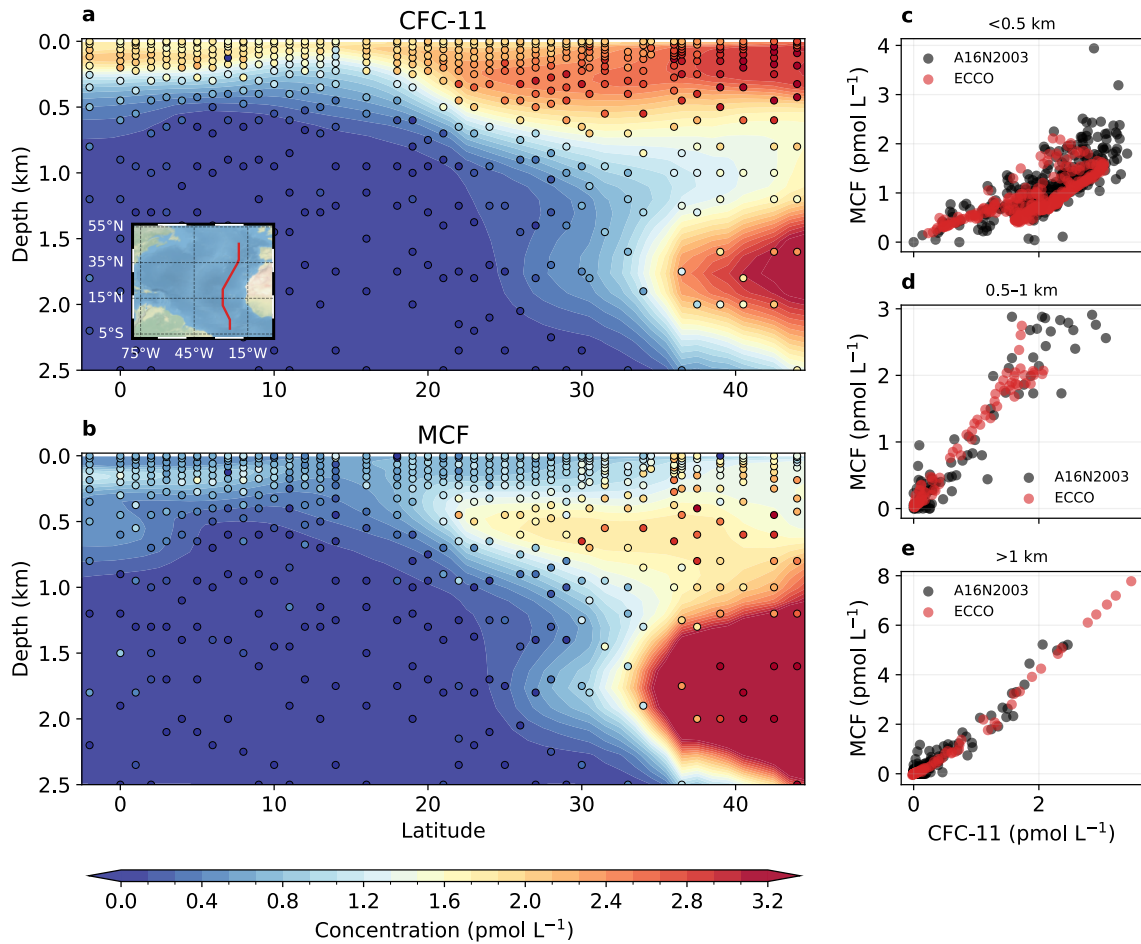
161 2.3 Quantifying changes in inferred OH associated with MCF air-sea fluxes

162 We estimate the amount of inferred OH required to account for the air-sea MCF fluxes
 163 using the following equation:

$$\frac{dB}{dt} \Big|_{ocn} = -k \cdot \Delta OH \cdot B \quad (1)$$

164 where B is the total atmospheric burden of MCF (in Gg, derived from observed atmospheric
 165 mole fractions [in parts per trillion; ppt] by applying a scaling factor of 23.57 Gg ppt⁻¹). This
 166 factor reflects the total atmospheric mass (5.1×10^{18} kg), along with the molar masses of air
 167 (28.96 g mol⁻¹) and MCF (133.4 g mol⁻¹). $\frac{dB}{dt} \Big|_{ocn}$ represents the rate of change in atmospheric
 168 MCF burden (in Gg yr⁻¹) due solely to air-sea exchange and is equivalent to the ocean uptake or
 169 outgassing of MCF. The reaction rate k corresponds to the temperature-dependent loss rate of
 170 MCF due to its reaction with OH, taken from Burkholder et al. (2019), assuming a mean
 171 tropospheric temperature of 266 K (as in Rigby et al., 2017). ΔOH represents the change in
 172 inferred OH that would be needed to account for the ocean-driven changes in atmospheric MCF
 173 burden. This approach requires only the total atmospheric MCF burden (can be derived from

174 observations) and the air-sea fluxes. Notably, it does not rely on MCF emission estimates, which
 175 are highly uncertain after 2000 (McCulloch & Midgley, 2001).



176

177 **Figure 1.** Validation of ECCO-simulated tracer distributions against observations. Panels **a** and **b** show
 178 vertical sections of CFC-11 and MCF concentrations along the A16N2003 cruise track. Observations are
 179 shown as colored dots and the cruise path is indicated by the red line in the map inset in panel **a**. ECCO
 180 July monthly mean concentrations in 2003 are shown as colored shading, averaged longitudinally from
 181 20° W to 29° W. Data below 2.5 km are omitted in **a,b** due to near-zero concentrations. Tracer-tracer
 182 scatter plots of observed and modeled CFC-11 versus MCF are shown in three depth ranges: above
 183 0.5 km (**c**), 0.5–1 km (**d**), and 1–6 km (**e**). Black dots represent observations; red dots show ECCO output
 184 sampled at the nearest horizontal grid point and vertically interpolated to the observed depth. The
 185 strong agreement between ECCO and observed values indicates that the model realistically captures
 186 ocean tracer uptake and distributions for both CFC-11 and MCF.

187 3 Results

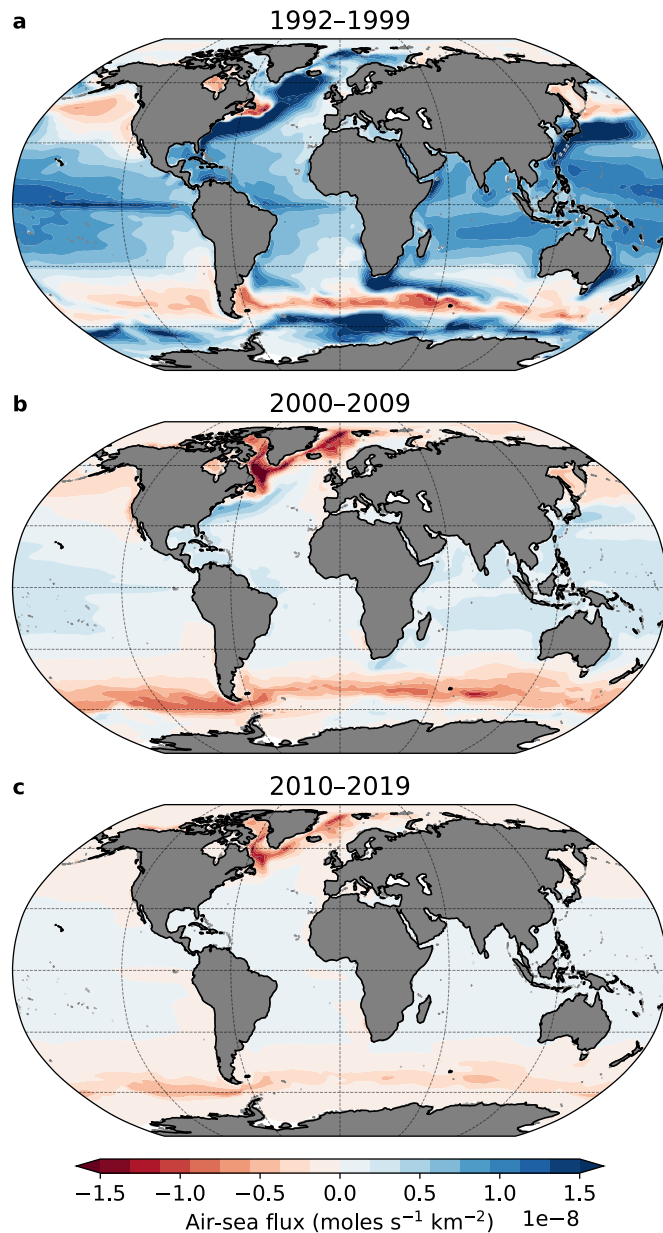
188 We first validate the ECCO simulation of ocean tracer uptake using CFC-11, which is a
 189 well-characterized and nearly conserved compound that has long served as a passive tracer for
 190 studying ocean circulation (e.g., Beismann & Redler, 2003; Bullister & Weiss, 1983; Dutay et al.,
 191 2002; England et al., 1994; Ito et al., 2004; Romanou et al., 2017; Wanninkhof, 1992, 2014;

192 Waugh, 2014). In this context, measured CFC-11, whose thermodynamic properties are well
193 known for estimating ocean physical uptake and was not used in the ECCO state estimation,
194 serves as independent evidence to test ECCO tracer uptake and distribution (Forget et al.,
195 2015b). Importantly, both MCF and CFC-11 were measured simultaneously along the A16N2003
196 cruise, enabling a consistent tracer-tracer comparison. Figure 1 presents both the absolute
197 concentrations and tracer-tracer scatter plots of CFC-11 and MCF from the ECCO simulation and
198 the A16N2003 observation. The model broadly captures the observed latitudinal and depth
199 distributions of both tracers, showing higher concentrations at high latitudes and in deeper
200 waters, where surface solubility is elevated (due to lower temperatures) and where deep-water
201 forms, facilitating tracer penetration.

202 The MCF results shown in Figure 1 represent our best estimate from the ECCO
203 simulation after updating two key parameters from W04: solubility and hydrolysis rate (see
204 Supplementary Text S1, S2 and Figure S4). Using the same freshwater solubility and hydrolysis
205 rate for MCF as in W04 would lead to an overestimation of ocean concentrations in the model
206 (Supplementary Figure S4 top row). However, updating the solubility based on a laboratory-
207 measured salting-out coefficient (Gossett, 1987), while keeping the hydrolysis rate unchanged,
208 shifts the modeled MCF concentrations toward the lower end of the observed range
209 (Supplementary Figure S4 middle row). However, we note that these hydrolysis losses of MCF
210 were primarily extracted from rates measured at temperatures between 25 °C and 120 °C
211 (Gerkens & Franklin, 1989), introducing substantial uncertainties in colder extratropical ocean
212 waters (Naus et al., 2021; Wennberg et al., 2004). We find better agreement between the
213 model and observations when the hydrolysis rate is reduced (i.e., slowed down), particularly at
214 colder temperatures. Note this adjusted hydrolysis rate remains well within the reported
215 uncertainty range (Gerkens & Franklin, 1989) (see Supplementary Figure S3).

216 Figure 2 shows ECCO-simulated spatial distributions of air-sea MCF fluxes over the past
217 three decades successively. In the 1990s, the global ocean acted predominantly as a sink for
218 MCF across most regions. Since the 2000s, however, the tropics have remained a sink while the
219 extratropical oceans are expected to have begun outgassing MCF. Intriguingly, this spatial flux
220 pattern is opposite to that of many other trace gases, such as CFC-11, HCFCs, HFCs, and CO₂,
221 which are typically taken up by the ocean at high latitudes and released to the atmosphere in
222 the tropics (DeVries et al., 2017; Gruber et al., 2009; Wang et al., 2021, 2023). This distinct
223 pattern for MCF is primarily driven by its strong temperature-dependent hydrolysis in the
224 ocean. Based on the hydrolysis parameters used in our simulation, MCF has a half-life on the
225 order of less than a year in warm tropical waters (~25 °C), but this extends to several decades in
226 extratropical oceans where sea surface temperature drops below 10 °C. As atmospheric MCF
227 concentrations have declined rapidly under the Montreal Protocol, the tropical ocean remains
228 undersaturated and continues to uptake MCF, due to rapid in situ degradation. In contrast, the

229 extratropics become oversaturated and outgas MCF because of much slower chemical loss in
 230 the surface ocean.

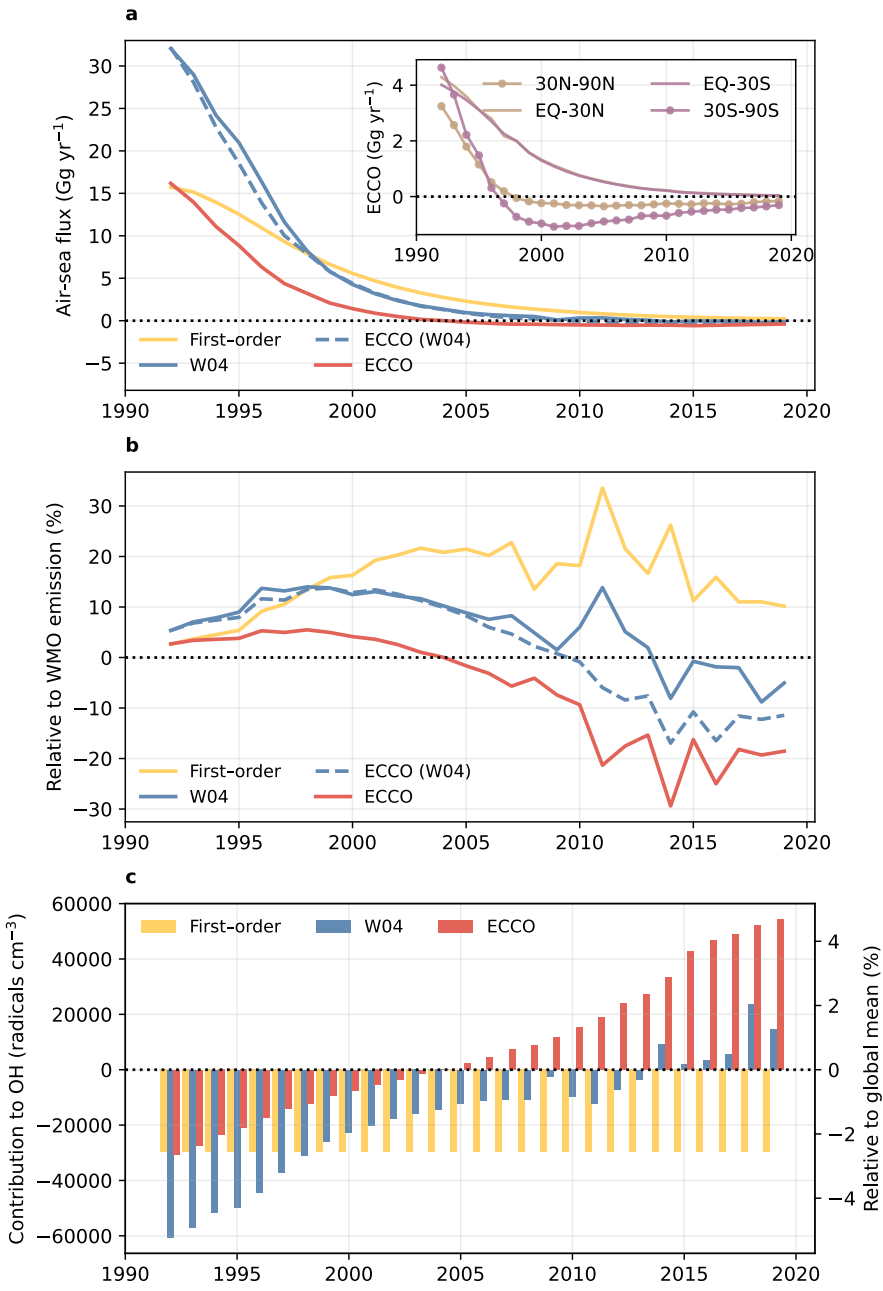


231

232 **Figure 2.** Spatial patterns of air-sea fluxes of MCF are shown as decadal averages for three time periods:
 233 1992–1999 (a), 2000–2009 (b), and 2010–2019 (c). Positive values (blue) indicate ocean uptake;
 234 negative values (red) indicate ocean outgassing.

235 To place our simulation in the context of earlier ocean representations, Figure 3a shows
 236 the globally integrated air-sea MCF flux for various ocean assumptions. Prior studies have often
 237 represented ocean uptake as a simple first-order loss process (e.g., assuming a constant oceanic
 238 partial lifetime of 197 years; Patra et al., 2011, 2014). Under this assumption, the oceanic loss in
 239 each year is calculated by simply dividing the atmospheric MCF burden by the oceanic partial

240 lifetime. This approach provides a reasonable approximation in the 1990s, when the global
 241 ocean acted as a net sink for MCF, and uptake was largely driven by high atmospheric MCF
 242 burden due to large anthropogenic emissions. However, as emissions declined rapidly after the
 243 1990s, the first-order loss assumption becomes increasingly inadequate, particularly in later
 244 years, because it assumes the ocean is always a net sink and does not account for the possibility
 245 of outgassing.



246

247 **Figure 3.** Time series of spatially integrated MCF air-sea fluxes and their impacts on inferred emissions
 248 and OH levels. Panel a shows comparison of global MCF air-sea fluxes from different ocean
 249 representations: first-order loss with an ocean partial lifetime of 197 years (yellow), an ocean general

250 circulation model used in W04 (blue), and ECCO simulations in this study. The ECCO run using the same
 251 freshwater solubility and hydrolysis rate as W04 is shown as the blue dashed line. The best estimate
 252 from ECCO — corrected for seawater solubility and with a slower cold-temperature hydrolysis rate — is
 253 shown as the red solid line. The inset panel in **a** shows the ECCO best estimate air-sea fluxes of MCF
 254 separately integrated over four latitude bands: 30° N–90° N, 30° N–equator, equator–30° S, and 30° S–
 255 90° S. Positive values indicate ocean uptake, and negative values indicate ocean outgassing. Panel **b**
 256 shows the same air-sea fluxes data in **a** but relative to top-down MCF emissions inferred in the WMO
 257 2022 Ozone Assessment report (Laube & Tegtmeier, 2022). Panel **c** shows the change in inferred OH
 258 that would be required to account for the air-sea MCF fluxes, if assuming the fluxes reflect changes in
 259 atmospheric MCF due to OH variations rather than atmosphere-ocean exchange (see Section 2.3 for
 260 details). The left y-axis indicates the absolute OH concentration (in radicals cm⁻³), and the right y-axis
 261 shows the corresponding relative change with respect to the global mean OH level of 1.16×10^6 radicals
 262 cm⁻³ (Spivakovsky et al., 2000).

263 The ECCO-simulated air-sea MCF flux, based on a time-varying ocean state, closely
 264 matches the W04 model, which uses a climatological ocean state, when the same freshwater
 265 solubility and hydrolysis rate parameters are applied (compare the blue solid and dashed lines
 266 in Figure 3**a**). This suggests that the oceanic MCF uptake is not strongly sensitive to the choice
 267 of ocean physical state. However, after accounting for seawater solubility and adopting a
 268 slower cold-temperature hydrolysis rate, the ocean acts as a significantly smaller reservoir for
 269 MCF — ocean uptake in the 1990s is reduced by more than 50%, and the onset of net
 270 outgassing occurs approximately five years in advance. This reduced ocean MCF uptake is
 271 driven primarily by the correction to seawater solubility, rather than adopting a slower
 272 hydrolysis rate, as demonstrated by additional sensitivity tests in Supplementary Figure S7.

273 Figure 3**b** compares the relative magnitude of various air-sea flux estimates to the top-
 274 down MCF emissions inferred in the World Meteorological Organization (WMO) 2022 Ozone
 275 Assessment report (Laube & Tegtmeier, 2022). In the 2010s, the inferred total MCF emissions
 276 were approximately 2.9 Gg yr⁻¹, even though reported consumption had dropped to zero (Rigby
 277 et al., 2017). While this estimated MCF emission relies on a climatological OH field (Rigby et al.,
 278 2013; Spivakovsky et al., 2000) — and the values may vary somewhat depending on the
 279 assumed OH levels — the ECCO simulation estimates suggest that the global ocean outgasses
 280 about 0.5 Gg yr⁻¹ of MCF back to the atmosphere, accounting for ~20% (and in some years up to
 281 30%) of the inferred total emissions during the same period. It is also important to note that
 282 the top-down estimates in Figure 3**b** are based on a first-order ocean loss with a partial lifetime
 283 of 94 years (Laube & Tegtmeier, 2022; Yvon-Lewis & Butler, 2002), which assumes the ocean
 284 continued to act as a net sink for MCF in the 2010s (at ~1.0 Gg yr⁻¹), despite the possibility that
 285 it had already become a net source. As a result, this inferred land-based MCF emission (Laube &
 286 Tegtmeier, 2022) can be largely overestimated (by up to 1.5 Gg yr⁻¹ in the 2010s).

287 Estimates of contributions to MCF-inferred OH due to different ocean representations
 288 are shown in Figure 3**c**. When the ocean acts as a net sink for MCF, accounting for air-sea fluxes
 289 lowers the inferred OH concentration because ocean uptake competes with OH as a sink for
 290 atmospheric MCF, reducing the amount of OH needed to balance the MCF mass budget. In
 291 contrast, when the ocean is a net source of MCF, including ocean outgassing increases the

292 inferred OH level, since more OH is required to remove the additional MCF released from the
293 ocean. To assess potential changes in inferred OH when using ECCO fluxes compared to earlier
294 ocean representations, if one assumes that the ocean uptakes more MCF or only weakly
295 outgasses MCF (e.g., W04 and first-order loss), but in reality the ocean uptakes less MCF before
296 2005 and outgasses more after 2005 (as simulated by ECCO), then the inferred OH levels would
297 be higher when using ECCO fluxes than when using W04 or first-order loss assumptions (by as
298 much as about 6% in recent years). Note that this estimated impact of switching ocean
299 representations on global mean OH assumes fixed emissions; part of the change in air-sea
300 fluxes could instead offset MCF emissions if emissions and OH were jointly optimized.

301 **4 Summary and Discussion**

302 We simulate MCF ocean uptake as accurately as current constraints allow — using an
303 ocean state estimate from ECCO and prescribed observed atmospheric MCF mole fractions. In
304 particular, by correcting for MCF seawater solubility as well as a slower cold-temperature
305 hydrolysis rate, our modeled ocean MCF concentrations show good agreement with depth-
306 resolved observations across a wide range of latitudes from a 2003 North Atlantic cruise. We
307 find that in the 2010s, ocean outgassing of MCF from ECCO ($\sim 0.5 \text{ Gg yr}^{-1}$) is substantially larger
308 than previous estimates, based either on simple first-order loss assumptions (which suggest
309 continued ocean uptake of up to $\sim 1 \text{ Gg yr}^{-1}$) or on a time-varying ocean flux from W04 (which
310 estimates outgassing at $\sim 0.03 \text{ Gg yr}^{-1}$). This is qualitatively consistent with a recent inversion
311 study (Naus et al., 2021), which suggested that a much larger high-latitude ocean source than
312 W04 is needed to explain the observed intra-hemispheric gradient in atmospheric MCF mole
313 fractions. Although the global ocean does not become a net source of MCF until after around
314 2005, the extratropical ocean appears to have begun outgassing as early as the late 1990s
315 (Figure 3a, insert panel). This raises the possibility that changes in atmospheric MCF mole
316 fractions previously attributed to European landfill emissions around the 2000s (Krol et al.,
317 2003; Reimann et al., 2005) may instead reflect contributions from the ocean, particularly given
318 that the subpolar North Atlantic emerges as a hot spot for ocean outgassing (Figure 2b,c).

319 As the observed decline in atmospheric MCF mole fractions slowed, previous inversion
320 models that relied on smaller ocean outgassing estimates compensated for this bias by
321 adjusting emissions to higher values, or invoking a decrease in atmospheric OH, or both, to
322 balance the MCF mass budget. In contrast, ECCO indicates a large ocean source of MCF,
323 potentially helping to explain the observed slowdown in the decay of atmospheric MCF mole
324 fractions without invoking a substantial OH decrease or persistent emissions. Most importantly,
325 our study suggests that the large MCF ocean source could account for as much as about 6% of
326 the 10–15% discrepancy between modelled and estimated absolute OH levels in recent years
327 (Naik et al., 2013; Prather et al., 2012; Prinn et al., 2005).

328 Future inversion studies — particularly with three-dimensional atmospheric models
329 (Naus et al., 2021; Patra et al., 2021) that incorporate spatially and temporally resolved MCF
330 air-sea fluxes from ECCO or other ocean reanalyses — could offer additional insights into the
331 spatiotemporal variability of OH. Such an approach would better disentangle oceanic and

anthropogenic MCF sources and provide estimates of absolute OH concentrations across latitudes. Notably, process-based chemistry-climate models tend to produce larger hemispheric OH ratios than those inferred from MCF-based inversions (Naik et al., 2013; Patra et al., 2014; Stevenson et al., 2020). Our results show that the Southern Hemisphere outgasses roughly twice as much MCF as the Northern Hemisphere, indicating that accounting for hemispheric asymmetries in ocean fluxes of MCF may substantially affect inferred interhemispheric OH distributions. Although estimates of Southern Ocean outgassing can carry large uncertainties due to both the challenges of modeling its complex ventilation (Dutay et al., 2002) and the paucity of direct oceanic MCF measurements in this region. Frequent low-pressure storms over the Southern Ocean can further complicate estimates by altering total barometric pressure and, in turn, influencing air-sea gas exchange (Kelly et al., 2025). Additionally, our study adjusted the MCF hydrolysis rate at cold temperatures beyond the range of existing laboratory measurements to improve agreement between the model and observations. Future work that directly measures MCF hydrolysis rates under ocean-relevant conditions would help reduce these uncertainties, particularly for high latitudes.

With the rapid decline in MCF emissions, which have become poorly constrained in recent decades, OH inversion studies are also exploring alternative tracers, such as HCFCs and HFCs (Liang et al., 2017), CO (Chen et al., 2025) and CO isotope (Krol et al., 2008; Morgenstern et al., 2025), formaldehyde (Wells et al., 2020; Wolfe et al., 2019), and methane (Penn et al., 2025). While promising, these substitutes face several limitations: shorter observational records than MCF, more complex source and sink processes beyond OH, and some methods offer only regional rather than global constraints on OH. Given these challenges, accurately characterizing OH levels inferred from MCF remains important, as it can provide a valuable benchmark for evaluating OH estimates derived from alternative tracers. Accounting for air-sea exchange of MCF is critical for improving the fidelity of OH inversions — especially in recent years, when ocean outgassing may constitute a substantial fraction of the total source and thus introduce biases in top-down estimates if this process is neglected or highly simplified.

359

360 Acknowledgments

361 P.W. gratefully acknowledges helpful discussions with Wei Chen, Qindan Zhu, and Gael Forget.
362 S.S. and P.W. acknowledge support from the National Science Foundation Atmospheric
363 Chemistry Division under grant 2128617. S.A.Y. acknowledges support from the CLIVAR repeat
364 hydrography program which is a joint effort between NOAA and NSF-OCE. M.R. received
365 funding from the UK Natural Environment Research Council Highlight Topic, InHALE
366 (Investigating HALocarbon impacts on the global Environment; NE/X00452X/1) and the NASA
367 Upper Atmosphere Research Program AGAGE grant 80NSSC21K1369. The computations
368 presented here were conducted using the “Svante” cluster, a facility located at MIT’s
369 Massachusetts Green High Performance Computing Center and supported by the Center for
370 Sustainability Science and Strategy (<https://cs3.mit.edu>).

371

372 **Open Research**

373 A16N2003 cruise data is available at <https://www.pmel.noaa.gov/co2/story/A16N>. AGAGE
374 atmospheric mole fractions data is available at <https://www-air.larc.nasa.gov/missions/agage/>.
375 Gridded ECCO monthly air-sea fluxes, ocean concentrations for CFC-11 and MCF, and code used
376 to generate all the figures in this analysis are available at Zenodo
377 (<https://doi.org/10.5281/zenodo.16648860>).
378

379 **References**

- 380 Beismann, J.-O., & Redler, R. (2003). Model simulations of CFC uptake in North Atlantic Deep
381 Water: Effects of parameterizations and grid resolution. *Journal of Geophysical
382 Research: Oceans*, 108(C5). <https://doi.org/10.1029/2001JC001253>
- 383 Bullister, J. L., & Weiss, R. F. (1983). Anthropogenic Chlorofluoromethanes in the Greenland and
384 Norwegian Seas. *Science*, 221(4607), 265–268.
385 <https://doi.org/10.1126/science.221.4607.265>
- 386 Bullister, John L., & Gruber, N. (2012). CRUISE REPORT: A16N_2003a [Data set].
387 https://cchdo.ucsd.edu/cruise/33RO200306_01
- 388 Burkholder, J. B., Sander, S. P., Abbatt, J., Barker J. R., Cappa, C., Crounse, J. D., Dibble, T. S.,
389 Huie, R. E., Kolb, C. E., Kurylo, M. J., Orkin, V. L., Percival, C. J., Wilmouth, D. M., and
390 Wine, P. H. Chemical Kinetics and Photochemical Data for Use in Atmospheric Studies,
391 Evaluation No. 19, JPL Publication 19-5, Jet Propulsion Laboratory, Pasadena, 2019
392 <http://jpldataeval.jpl.nasa.gov>.
- 393 Butler, J. H., Elkins, J. W., Thompson, T. M., Hall, B. D., Swanson, T. H., & Koropalov, V. (1991).
394 Oceanic consumption of CH₃CCl₃: Implications for tropospheric OH. *Journal of
395 Geophysical Research: Atmospheres*, 96(D12), 22347–22355.
396 <https://doi.org/10.1029/91JD02126>
- 397 Chen, W., Zhang, Y., & Liang, R. (2025). Converging evidence for reduced global atmospheric
398 oxidation in 2020. *National Science Review*, nwaf232.
399 <https://doi.org/10.1093/nsr/nwaf232>
- 400 DeVries, T., Holzer, M., & Primeau, F. (2017). Recent increase in oceanic carbon uptake driven
401 by weaker upper-ocean overturning. *Nature*, 542(7640), 215–218.
402 <https://doi.org/10.1038/nature21068>
- 403 Dutay, J.-C., Bullister, J. L., Doney, S. C., Orr, J. C., Najjar, R., Caldeira, K., et al. (2002). Evaluation
404 of ocean model ventilation with CFC-11: comparison of 13 global ocean models. *Ocean
405 Modelling*, 4(2), 89–120.
- 406 England, M. H., Garçon, V., & Minster, J.-F. (1994). Chlorofluorocarbon uptake in a world ocean
407 model: 1. Sensitivity to the surface gas forcing. *Journal of Geophysical Research: Oceans*,
408 99(C12), 25215–25233. <https://doi.org/10.1029/94JC02205>

- 409 Forget, G., Campin, J.-M., Heimbach, P., Hill, C. N., Ponte, R. M., & Wunsch, C. (2015a). ECCO
410 version 4: an integrated framework for non-linear inverse modeling and global ocean
411 state estimation. *Geoscientific Model Development*, 8(10), 3071–3104.
412 <https://doi.org/10.5194/gmd-8-3071-2015>
- 413 Forget, G., Ferreira, D., & Liang, X. (2015b). On the observability of turbulent transport rates by
414 Argo: supporting evidence from an inversion experiment. *Ocean Science*, 11(5), 839–
415 853. <https://doi.org/10.5194/os-11-839-2015>
- 416 Gerkens, R. R., & Franklin, J. A. (1989). The rate of degradation of 1,1,1-trichloroethane in water
417 by hydrolysis and dehydrochlorination. *Chemosphere*, 19(12), 1929–1937.
418 [https://doi.org/10.1016/0045-6535\(89\)90016-7](https://doi.org/10.1016/0045-6535(89)90016-7)
- 419 Gossett, J. M. (1987). Measurement of Henry's law constants for C1 and C2 chlorinated
420 hydrocarbons. *Environmental Science & Technology*, 21(2), 202–208.
421 <https://doi.org/10.1021/es00156a012>
- 422 Gruber, N., Gloor, M., Mikaloff Fletcher, S. E., Doney, S. C., Dutkiewicz, S., Follows, M. J., et al.
423 (2009). Oceanic sources, sinks, and transport of atmospheric CO₂. *Global
424 Biogeochemical Cycles*, 23(1). <https://doi.org/10.1029/2008GB003349>
- 425 Ito, T., Marshall, J., & Follows, M. (2004). What controls the uptake of transient tracers in the
426 Southern Ocean? *Global Biogeochemical Cycles*, 18(2).
- 427 Kelly, C. L., Chang, B. X., Emmanuelli, A. F., Park, E. R., Macdonald, A. M., & Nicholson, D. P.
428 (2025, April 30). Low-pressure storms drive nitrous oxide emissions in the Southern
429 Ocean. Research Square. <https://doi.org/10.21203/rs.3.rs-6378208/v1>
- 430 Krol, M., & Lelieveld, J. (2003). Can the variability in tropospheric OH be deduced from
431 measurements of 1,1,1-trichloroethane (methyl chloroform)? *Journal of Geophysical
432 Research: Atmospheres*, 108(D3). <https://doi.org/10.1029/2002JD002423>
- 433 Krol, M. C., Lelieveld, J., Oram, D. E., Sturrock, G. A., Penkett, S. A., Brenninkmeijer, C. A. M., et
434 al. (2003). Continuing emissions of methyl chloroform from Europe. *Nature*, 421(6919),
435 131–135. <https://doi.org/10.1038/nature01311>
- 436 Krol, M. C., Meirink, J. F., Bergamaschi, P., Mak, J. E., Lowe, D., Jöckel, P., et al. (2008). What can
437 ¹⁴CO measurements tell us about OH? *Atmospheric Chemistry and Physics*, 8(16), 5033–
438 5044. <https://doi.org/10.5194/acp-8-5033-2008>
- 439 Laube, J. C., & Tegtmeier, S. (2022). *Scientific Assessment of Ozone Depletion: 2022. Chapter 1:
440 Update on Ozone-Depleting Substances (ODSs) and Other Gases of Interest to the
441 Montreal Protocol* (No. 278) (p. 509). Geneva, Switzerland: World Meteorological
442 Organization.
- 443 Levy, H. (1971). Normal Atmosphere: Large Radical and Formaldehyde Concentrations
444 Predicted. *Science*, 173(3992), 141–143. <https://doi.org/10.1126/science.173.3992.141>
- 445 Liang, Q., Chipperfield, M. P., Fleming, E. L., Abraham, N. L., Braesicke, P., Burkholder, J. B., et al.
446 (2017). Deriving Global OH Abundance and Atmospheric Lifetimes for Long-Lived Gases:

- 447 A Search for CH₃CCl₃ Alternatives. *Journal of Geophysical Research: Atmospheres*,
448 122(21), 11,914–11,933. <https://doi.org/10.1002/2017JD026926>
- 449 Marshall, J., Adcroft, A., Hill, C., Perelman, L., & Heisey, C. (1997a). A finite-volume,
450 incompressible Navier Stokes model for studies of the ocean on parallel computers.
451 *Journal of Geophysical Research: Oceans*, 102(C3), 5753–5766.
- 452 Marshall, J., Hill, C., Perelman, L., & Adcroft, A. (1997b). Hydrostatic, quasi-hydrostatic, and
453 nonhydrostatic ocean modeling. *Journal of Geophysical Research: Oceans*, 102(C3),
454 5733–5752.
- 455 McCulloch, A., & Midgley, P. M. (2001). The history of methyl chloroform emissions: 1951–
456 2000. *Atmospheric Environment*, 35(31), 5311–5319. <https://doi.org/10.1016/S1352->
457 2310(01)00306-5
- 458 McNorton, J., Chipperfield, M. P., Gloor, M., Wilson, C., Feng, W., Hayman, G. D., et al. (2016).
459 Role of OH variability in the stalling of the global atmospheric CH₄ growth rate from
460 1999 to 2006. *Atmospheric Chemistry and Physics*, 16(12), 7943–7956.
461 <https://doi.org/10.5194/acp-16-7943-2016>
- 462 Montzka, S. A., Krol, M., Dlugokencky, E., Hall, B., Jöckel, P., & Lelieveld, J. (2011). Small
463 Interannual Variability of Global Atmospheric Hydroxyl. *Science*, 331(6013), 67–69.
464 <https://doi.org/10.1126/science.1197640>
- 465 Morgenstern, O., Moss, R., Manning, M., Zeng, G., Schaefer, H., Usoskin, I., et al. (2025).
466 Radiocarbon monoxide indicates increasing atmospheric oxidizing capacity. *Nature
467 Communications*, 16(1), 249. <https://doi.org/10.1038/s41467-024-55603-1>
- 468 Murray, L. T., Fiore, A. M., Shindell, D. T., Naik, V., & Horowitz, L. W. (2021). Large uncertainties
469 in global hydroxyl projections tied to fate of reactive nitrogen and carbon. *Proceedings
470 of the National Academy of Sciences*, 118(43), e2115204118.
471 <https://doi.org/10.1073/pnas.2115204118>
- 472 Naik, V., Voulgarakis, A., Fiore, A. M., Horowitz, L. W., Lamarque, J.-F., Lin, M., et al. (2013).
473 Preindustrial to present-day changes in tropospheric hydroxyl radical and methane
474 lifetime from the Atmospheric Chemistry and Climate Model Intercomparison Project
475 (ACCMIP). *Atmospheric Chemistry and Physics*, 13(10), 5277–5298.
476 <https://doi.org/10.5194/acp-13-5277-2013>
- 477 Naus, S., Montzka, S. A., Pandey, S., Basu, S., Dlugokencky, E. J., & Krol, M. (2019). Constraints
478 and biases in a tropospheric two-box model of OH. *Atmospheric Chemistry and Physics*,
479 19(1), 407–424. <https://doi.org/10.5194/acp-19-407-2019>
- 480 Naus, S., Montzka, S. A., Patra, P. K., & Krol, M. C. (2021). A three-dimensional-model inversion
481 of methyl chloroform to constrain the atmospheric oxidative capacity. *Atmospheric
482 Chemistry and Physics*, 21(6), 4809–4824. <https://doi.org/10.5194/acp-21-4809-2021>
- 483 Nicely, J. M., Duncan, B. N., Hanisco, T. F., Wolfe, G. M., Salawitch, R. J., Deushi, M., et al.
484 (2020). A machine learning examination of hydroxyl radical differences among model

- 485 simulations for CCM1-1. *Atmospheric Chemistry and Physics*, 20(3), 1341–1361.
486 <https://doi.org/10.5194/acp-20-1341-2020>
- 487 Patra, P. K., Houweling, S., Krol, M., Bousquet, P., Belikov, D., Bergmann, D., et al. (2011).
488 TransCom model simulations of CH₄ and related species: linking transport, surface flux
489 and chemical loss with CH₄ variability in the troposphere and lower stratosphere.
490 *Atmospheric Chemistry and Physics*, 11(24), 12813–12837. <https://doi.org/10.5194/acp-11-12813-2011>
- 492 Patra, P. K., Krol, M. C., Montzka, S. A., Arnold, T., Atlas, E. L., Lintner, B. R., et al. (2014).
493 Observational evidence for interhemispheric hydroxyl-radical parity. *Nature*, 513(7517),
494 219–223. <https://doi.org/10.1038/nature13721>
- 495 Patra, P. K., Krol, M. C., Prinn, R. G., Takigawa, M., Mühle, J., Montzka, S. A., et al. (2021).
496 Methyl Chloroform Continues to Constrain the Hydroxyl (OH) Variability in the
497 Troposphere. *Journal of Geophysical Research: Atmospheres*, 126(4), e2020JD033862.
498 <https://doi.org/10.1029/2020JD033862>
- 499 Penn, E., Jacob, D. J., Chen, Z., East, J. D., Sulprizio, M. P., Bruhwiler, L., et al. (2025). What can
500 we learn about tropospheric OH from satellite observations of methane? *Atmospheric
501 Chemistry and Physics*, 25(5), 2947–2965. <https://doi.org/10.5194/acp-25-2947-2025>
- 502 Prather, M., & Spivakovsky, C. M. (1990). Tropospheric OH and the lifetimes of
503 hydrochlorofluorocarbons. *Journal of Geophysical Research: Atmospheres*, 95(D11),
504 18723–18729. <https://doi.org/10.1029/JD095iD11p18723>
- 505 Prather, M. J., Holmes, C. D., & Hsu, J. (2012). Reactive greenhouse gas scenarios: Systematic
506 exploration of uncertainties and the role of atmospheric chemistry. *Geophysical
507 Research Letters*, 39(9). <https://doi.org/10.1029/2012GL051440>
- 508 Prinn, R., Cunnold, D., Simmonds, P., Alyea, F., Boldi, R., Crawford, A., et al. (1992). Global
509 average concentration and trend for hydroxyl radicals deduced from ALE/GAGE
510 trichloroethane (methyl chloroform) data for 1978–1990. *Journal of Geophysical
511 Research: Atmospheres*, 97(D2), 2445–2461. <https://doi.org/10.1029/91JD02755>
- 512 Prinn, R. G., Huang, J., Weiss, R. F., Cunnold, D. M., Fraser, P. J., Simmonds, P. G., et al. (2005).
513 Evidence for variability of atmospheric hydroxyl radicals over the past quarter century.
514 *Geophysical Research Letters*, 32(7). <https://doi.org/10.1029/2004GL022228>
- 515 Prinn, Ronald G, Weiss, R. F., Arduini, J., Arnold, T., DeWitt, H. L., Fraser, P. J., et al. (2018).
516 History of chemically and radiatively important atmospheric gases from the Advanced
517 Global Atmospheric Gases Experiment (AGAGE). *Earth System Science Data*, 10(2), 985–
518 1018.
- 519 Reimann, S., Manning, A. J., Simmonds, P. G., Cunnold, D. M., Wang, R. H. J., Li, J., et al. (2005).
520 Low European methyl chloroform emissions inferred from long-term atmospheric
521 measurements. *Nature*, 433(7025), 506–508. <https://doi.org/10.1038/nature03220>
- 522 Rigby, M., Prinn, R. G., O'Doherty, S., Montzka, S. A., McCulloch, A., Harth, C. M., et al. (2013).
523 Re-evaluation of the lifetimes of the major CFCs and CH₃CCl₃ using atmospheric trends.

- 524 *Atmospheric Chemistry and Physics*, 13(5), 2691–2702. <https://doi.org/10.5194/acp-13-2691-2013>
- 525
- 526 Rigby, Matthew, Montzka, S. A., Prinn, R. G., White, J. W. C., Young, D., O'Doherty, S., et al.
527 (2017). Role of atmospheric oxidation in recent methane growth. *Proceedings of the
528 National Academy of Sciences*, 114(21), 5373–5377.
529 <https://doi.org/10.1073/pnas.1616426114>
- 530 Romanou, A., Marshall, J., Kelley, M., & Scott, J. (2017). Role of the ocean's AMOC in setting the
531 uptake efficiency of transient tracers. *Geophysical Research Letters*, 44(11), 5590–5598.
- 532 Singh, H. B., Kanakidou, M., Crutzen, P. J., & Jacob, D. J. (1995). High concentrations and
533 photochemical fate of oxygenated hydrocarbons in the global troposphere. *Nature*,
534 378(6552), 50–54. <https://doi.org/10.1038/378050a0>
- 535 Spivakovsky, C. M., Logan, J. A., Montzka, S. A., Balkanski, Y. J., Foreman-Fowler, M., Jones, D. B.
536 A., et al. (2000). Three-dimensional climatological distribution of tropospheric OH:
537 Update and evaluation. *Journal of Geophysical Research: Atmospheres*, 105(D7), 8931–
538 8980. <https://doi.org/10.1029/1999JD901006>
- 539 Stevenson, D. S., Zhao, A., Naik, V., O'Connor, F. M., Tilmes, S., Zeng, G., et al. (2020). Trends in
540 global tropospheric hydroxyl radical and methane lifetime since 1850 from
541 AerChemMIP. *Atmospheric Chemistry and Physics*, 20(21), 12905–12920.
542 <https://doi.org/10.5194/acp-20-12905-2020>
- 543 Turner, A. J., Frankenberg, C., Wennberg, P. O., & Jacob, D. J. (2017). Ambiguity in the causes
544 for decadal trends in atmospheric methane and hydroxyl. *Proceedings of the National
545 Academy of Sciences*, 114(21), 5367–5372. <https://doi.org/10.1073/pnas.1616020114>
- 546 Wang, P., Scott, J. R., Solomon, S., Marshall, J., Babbin, A. R., Lickley, M., et al. (2021). On the
547 effects of the ocean on atmospheric CFC-11 lifetimes and emissions. *Proceedings of the
548 National Academy of Sciences*, 118(12), e2021528118.
549 <https://doi.org/10.1073/pnas.2021528118>
- 550 Wang, P., Solomon, S., Lickley, M., Scott, J. R., Weiss, R. F., & Prinn, R. G. (2023). On the
551 Influence of Hydroxyl Radical Changes and Ocean Sinks on Estimated HCFC and HFC
552 Emissions and Banks. *Geophysical Research Letters*, 50(18), e2023GL105472.
553 <https://doi.org/10.1029/2023GL105472>
- 554 Wanninkhof, R. (1992). Relationship between wind speed and gas exchange over the ocean.
555 *Journal of Geophysical Research: Oceans*, 97(C5), 7373–7382.
556 <https://doi.org/10.1029/92JC00188>
- 557 Wanninkhof, R. (2014). Relationship between wind speed and gas exchange over the ocean
558 revisited. *Limnology and Oceanography: Methods*, 12(6), 351–362.
559 <https://doi.org/10.4319/lom.2014.12.351>
- 560 Waugh, D. W. (2014). Changes in the ventilation of the southern oceans. *Philosophical
561 Transactions of the Royal Society A: Mathematical, Physical and Engineering Sciences*,
562 372(2019), 20130269. <https://doi.org/10.1098/rsta.2013.0269>

- 563 Wells, K. C., Millet, D. B., Payne, V. H., Deventer, M. J., Bates, K. H., de Gouw, J. A., et al. (2020).
564 Satellite isoprene retrievals constrain emissions and atmospheric oxidation. *Nature*,
565 585(7824), 225–233. <https://doi.org/10.1038/s41586-020-2664-3>
- 566 Wennberg, P. O., Peacock, S., Randerson, J. T., & Bleck, R. (2004). Recent changes in the air-sea
567 gas exchange of methyl chloroform. *Geophysical Research Letters*, 31(16).
568 <https://doi.org/10.1029/2004GL020476>
- 569 Wolfe, G. M., Nicely, J. M., St. Clair, J. M., Hanisco, T. F., Liao, J., Oman, L. D., et al. (2019).
570 Mapping hydroxyl variability throughout the global remote troposphere via synthesis of
571 airborne and satellite formaldehyde observations. *Proceedings of the National Academy
572 of Sciences*, 116(23), 11171–11180. <https://doi.org/10.1073/pnas.1821661116>
- 573 Yvon-Lewis, S. A., & Butler, J. H. (2002). Effect of oceanic uptake on atmospheric lifetimes of
574 selected trace gases. *Journal of Geophysical Research: Atmospheres*, 107(D20), ACH 1-1-
575 ACH 1-9. <https://doi.org/10.1029/2001JD001267>
- 576 Yvon-Lewis, S. A., King, D. B., Tokarczyk, R., Goodwin, K. D., Saltzman, E. S., & Butler, J. H.
577 (2004). Methyl bromide and methyl chloride in the Southern Ocean. *Journal of
578 Geophysical Research: Oceans*, 109(C2). <https://doi.org/10.1029/2003JC001809>
- 579 Zhu, Q., Fiore, A. M., Correa, G., Lamarque, J.-F., & Worden, H. (2024). The impact of internal
580 climate variability on OH trends between 2005 and 2014. *Environmental Research
581 Letters*, 19(6), 064032. <https://doi.org/10.1088/1748-9326/ad4b47>
- 582

Ocean Outgassing of Methyl Chloroform as an Underestimated Source of Emission

Peidong Wang^{1*}, Susan Solomon¹, Jeffery R. Scott¹, Shari A. Yvon-Lewis², Paul O. Wennberg³, Ray F. Weiss⁴, Matthew Rigby^{5,6}, Minde An⁶

¹Department of Earth, Atmospheric and Planetary Sciences, Massachusetts Institute of Technology, Cambridge, MA, USA.

²Department of Oceanography, Texas A&M University, College Station, TX, USA.

³Division of Geological and Planetary Sciences, California Institute of Technology, Pasadena, CA, USA.

⁴Scripps Institution of Oceanography, University of California San Diego, La Jolla, CA, USA.

⁵School of Chemistry, University of Bristol, Bristol, UK.

⁶Center for Sustainability Science and Strategy, Massachusetts Institute of Technology, Cambridge, MA, USA.

Contents of this file

Text S1 to S3

Figures S1 to S7

Tables S1

Introduction

The supporting information contains text descriptions of ECCO model parameterizations and 7 figures supplementary to the main figures. It also has 1 supplementary table showing the solubility parameters for MCF used in ECCO.

Text S1. Air-sea exchange parameterization

We use the gas exchange velocity parameterization $k = 0.251 U^2 (Sc/660)^{-0.5}$ from (Wanninkhof, 2014), which updates the coefficient from the earlier value of 0.31 used in (Wanninkhof, 1992). Here, U is the wind speed, and Sc is the Schmidt number, representing the ratio of the kinematic viscosity of seawater to the molecular diffusivity of the gas. For CFC-11, we use the seawater Schmidt number coefficients provided in (Wanninkhof, 2014). For MCF, whose molecular diffusivity is 0.8 times that of CFC-11 (Butler et al., 1991), we scale its Schmidt number by a factor of 1.25 (1/0.8) relative to CFC-11.

Following W04, we calculate MCF solubility using the Henry's law constant for freshwater (Gossett, 1987):

$$H = 10^{-3} \exp\left(-9.777 + \frac{4133}{T}\right) \quad [1]$$

where H is the temperature-dependent freshwater solubility in units of mol atm⁻¹ L⁻¹, and T is the temperature in Kelvin. To convert freshwater solubility to seawater solubility, we apply the Setschenow relationship using the measured salting-out coefficient $K_s = 0.193$ from (Gossett, 1987):

$$H_{sw} = H 10^{-K_s \frac{S}{M_{NaCl}}} \quad [2]$$

where H_{sw} is the seawater solubility (mol atm⁻¹ L⁻¹), S is salinity in g L⁻¹, and M_{NaCl} is the molar mass of sodium chloride (58.44 g mol⁻¹). We then fit the temperature- and salinity-dependent MCF solubility to the polynomial form used in the ECCO code. The fitted coefficients for MCF and CFC-11 (directly obtained from Warner & Weiss, 1985) are listed in Supplementary Table S1.

Text S2. MCF hydrolysis parameterization

MCF is degraded in the ocean via hydrolysis, with a rate constant k (units in s⁻¹) given by:

$$\log_{10} k = \log_{10} A - \frac{E}{2.303 R T} \quad [3]$$

where $\log_{10} A = 13.1 \pm 0.8$ (with the frequency factor A in units of s⁻¹) and $E = 117.8 \pm 5.2$ kJ mol⁻¹ (activation energy), based on laboratory measurements (Gerkens & Franklin, 1989). The gas constant $R = 8.314 \times 10^{-3}$ kJ mol⁻¹ K⁻¹, and T is the temperature in Kelvin. This hydrolysis rate is used in W04 as well. The corresponding hydrolysis half-life is shown in Supplementary Figure S3, with blue shading indicating the reported uncertainties. However, these rate constants are derived from temperatures between 25 °C and 120 °C, making their application to the cold extratropical ocean highly extrapolated. As shown in Supplementary Figure S4 (middle row), applying this hydrolysis rate leads to an underestimation of MCF concentrations in ECCO, particularly above 500 m. To better match observations, we adopt revised parameters of $\log_{10} A = 22.5$ and $E = 170.7$, shown as the red line in Supplementary Figure S3. This adjustment steepens the temperature dependence of k , maintaining a similar hydrolysis rate around 20 °C but slowing down the rate at colder temperatures. While the adjusted values lie

well outside the individual uncertainty ranges for A and E reported in (Gerkens & Franklin, 1989), the resulting rate constant k remains within the original uncertainty envelope for ocean-relevant temperatures (2 to 35 °C).

Text S3. ECCO tracer diffusivity parameterization

It has been suggested that ECCO may underestimate diapycnal diffusivity between approximately 200 m and 1,500 m depth (Trossman et al., 2022), although other physical processes may also influence turbulent mixing (Forget et al., 2015). To address this, we enhanced the vertical diffusivity only for passive tracers (CFC-11 and MCF) by adding a uniform constant of $2 \times 10^{-5} \text{ m}^2 \text{ s}^{-1}$ between 65 m and 1,515 m. Note that this approach does not alter the ocean's physical circulation in ECCO. The adjustment improves the agreement between simulated and observed absolute CFC-11 concentrations along the A16N2003 transect, especially above 1,500 m depth (see Supplementary Figure S5). All results presented in this study are based on simulations with the enhanced tracer diffusivity. We note that this adjustment in tracer diffusivity has a minimal impact on the global ocean uptake of MCF, as shown in Supplementary Figure S6.

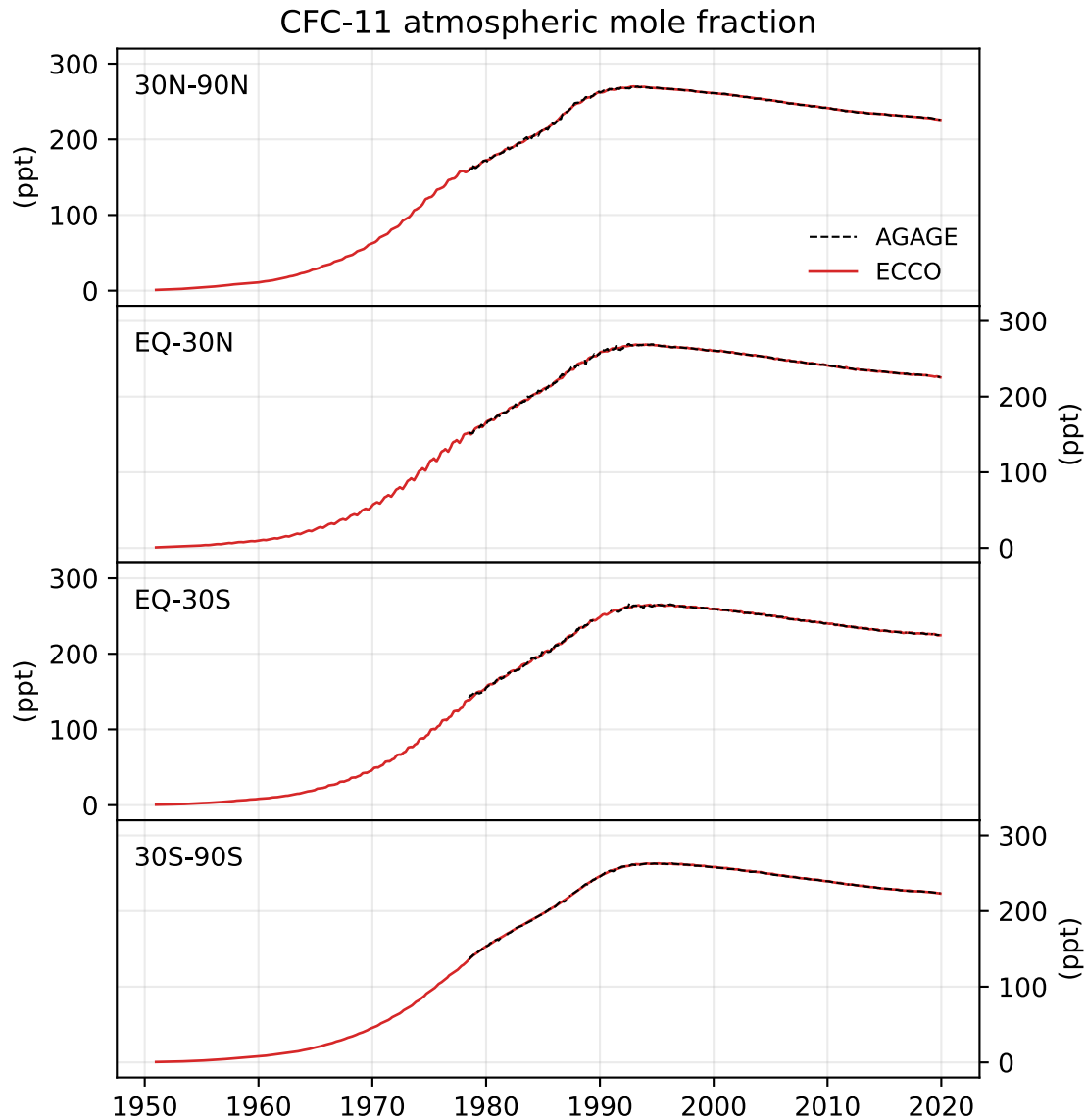


Figure S1. Atmospheric mole fractions of CFC-11 used in ECCO. Red lines show the monthly atmospheric mole fractions from the 12-box model output for CFC-11, which are prescribed in ECCO at four latitude bands: 30° N– 90° N, 30° N–equator, equator– 30° S, and 30° S– 90° S from 1951 to 2019. Black dashed lines indicate monthly AGAGE observations, available from 1978 onward, for comparison.

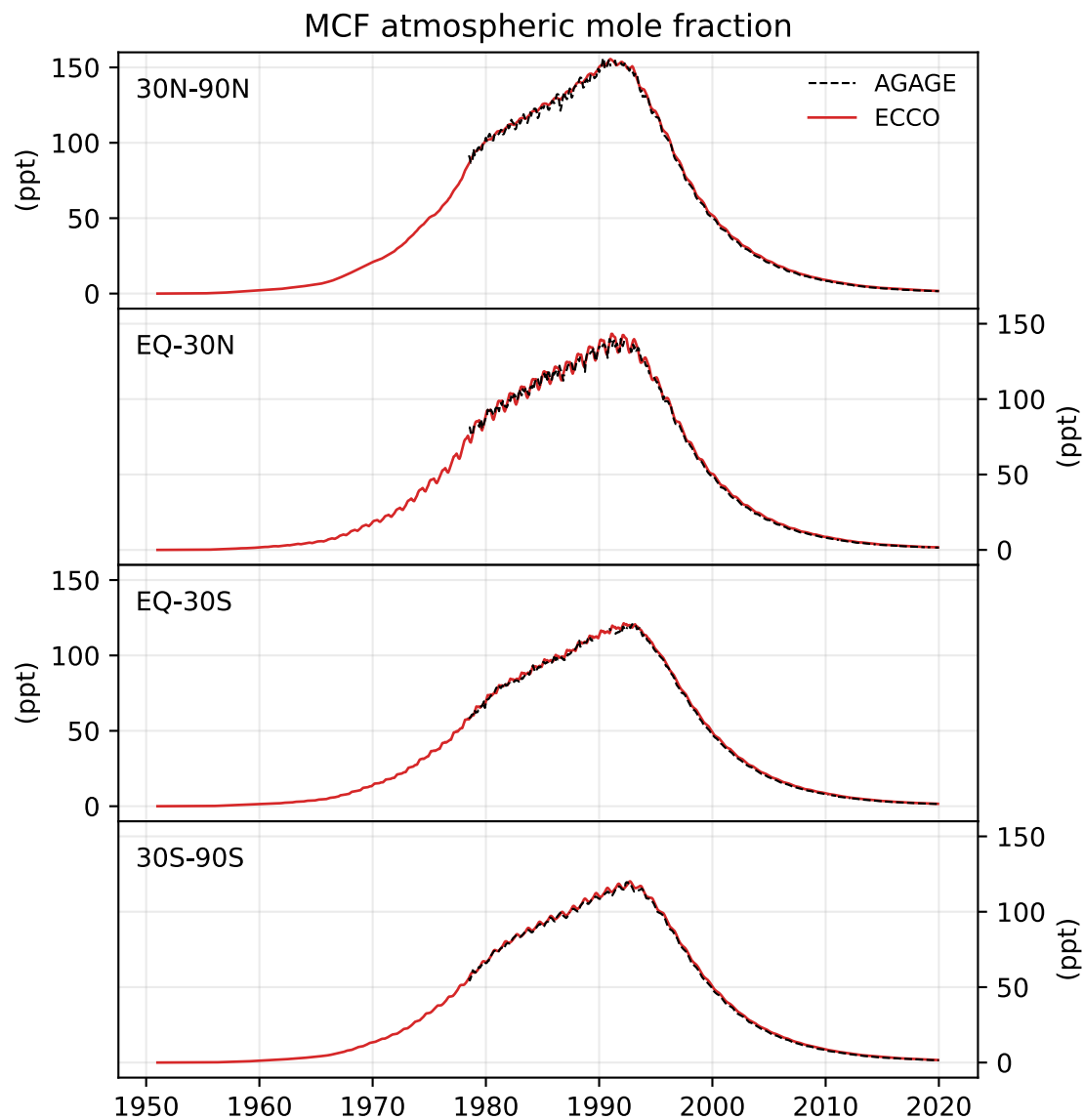


Figure S2. Similar as Figure S1, but for MCF.

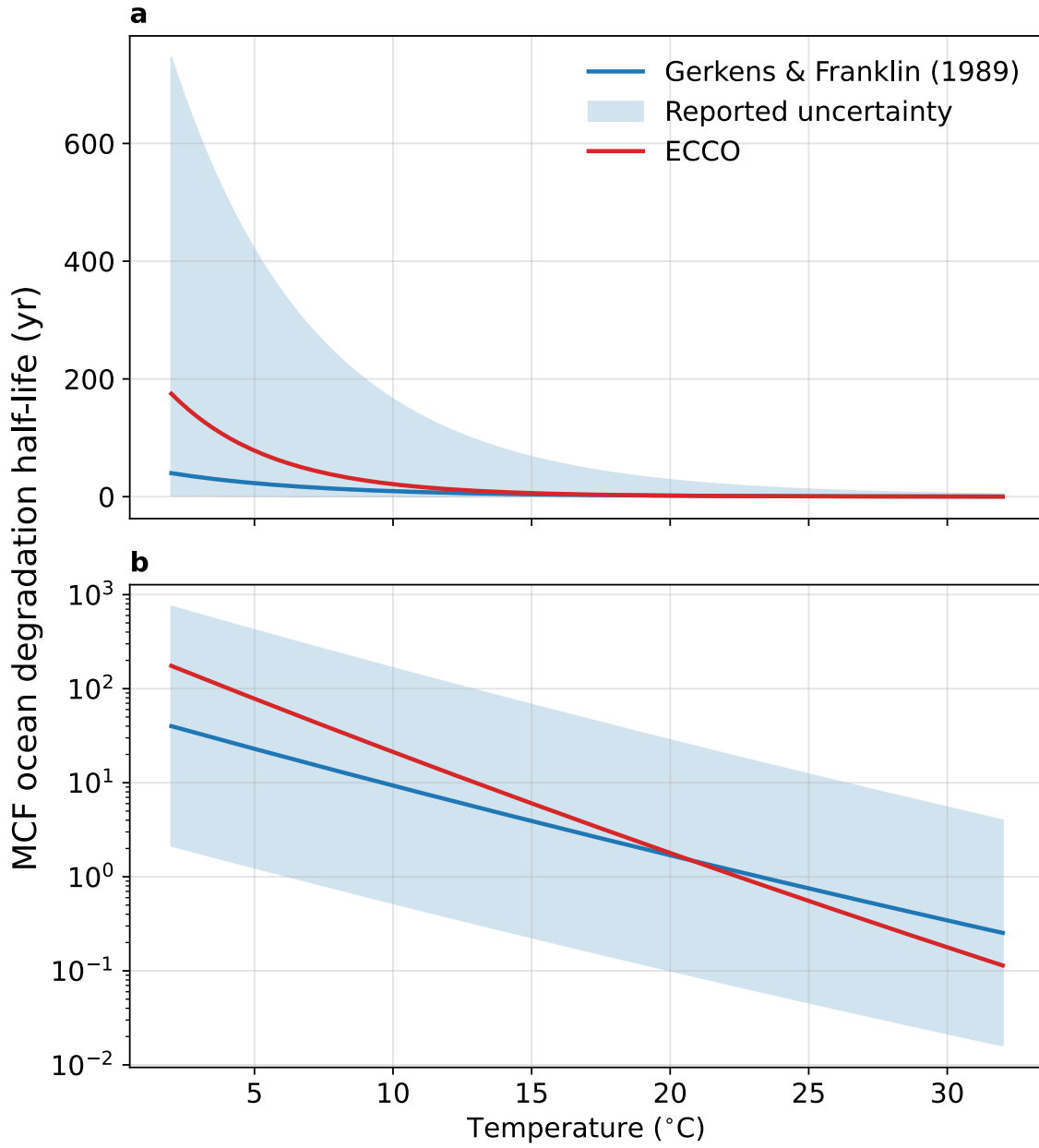


Figure S3. The solid blue line shows the temperature-dependent half-life of MCF hydrolysis based on parameters from (Gerkens & Franklin, 1989; also used in W04), with shaded areas indicating the reported uncertainty range. The red line represents the hydrolysis rate used in the ECCO simulation. Both panels show the same data, except panel **a** uses a linear scale, while panel **b** uses a logarithmic scale to facilitate comparison.

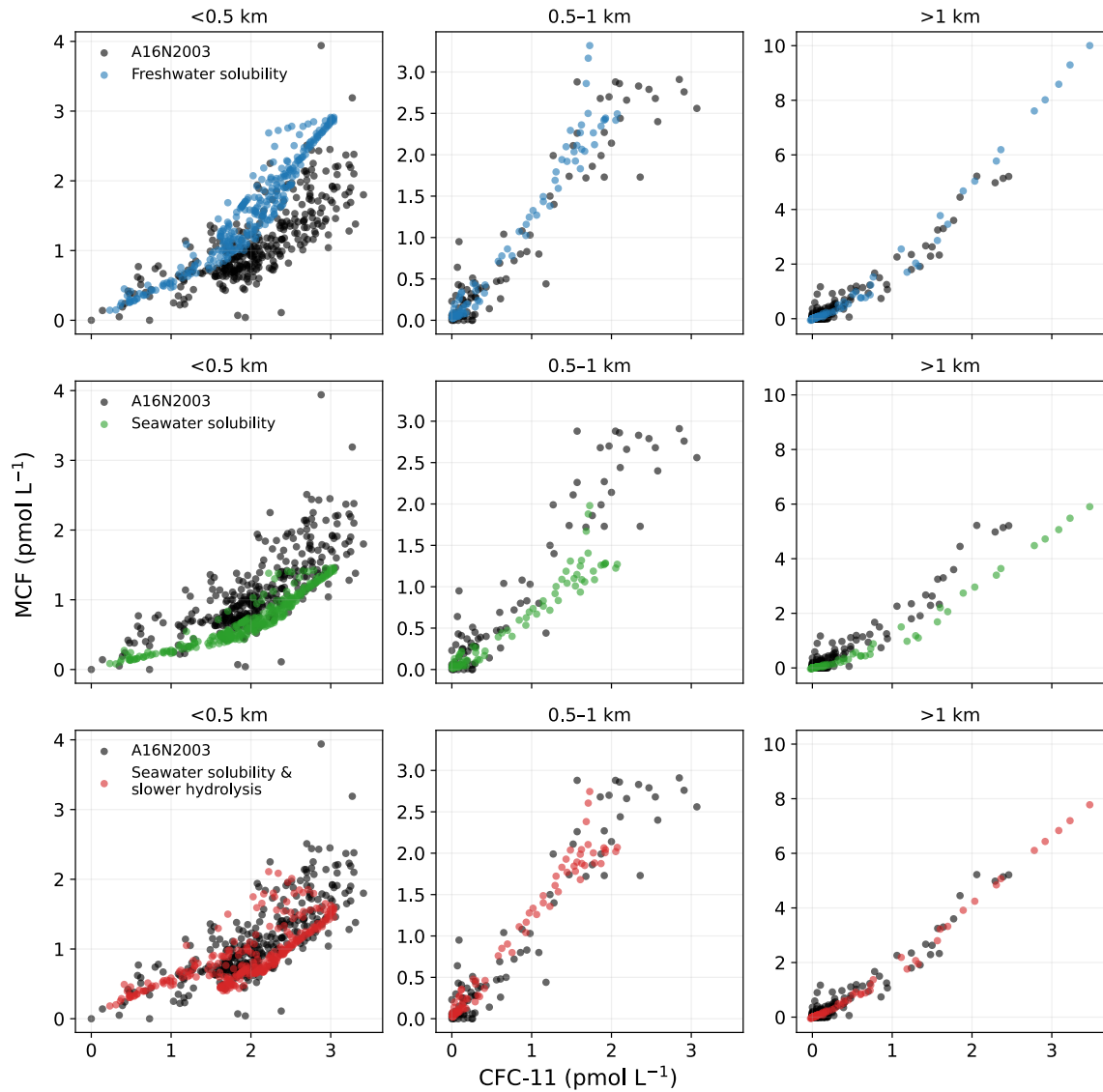


Figure S4. Tracer-tracer model-data comparison. Similar to Figure 1 panels c,d,e, showing tracer-tracer scatter plots of CFC-11 versus MCF from observations (black dots; same across columns) and co-located ECCO simulations (colored dots). Different depth ranges are shown across columns. Top row (blue dots): ECCO simulations using the same freshwater solubility and hydrolysis rates from W04. Middle row (green dots): simulations using seawater solubility while using the same hydrolysis rate as in W04. Bottom row (red dots): simulations using seawater solubility and a slower hydrolysis rate, same data shown in Figure 1.

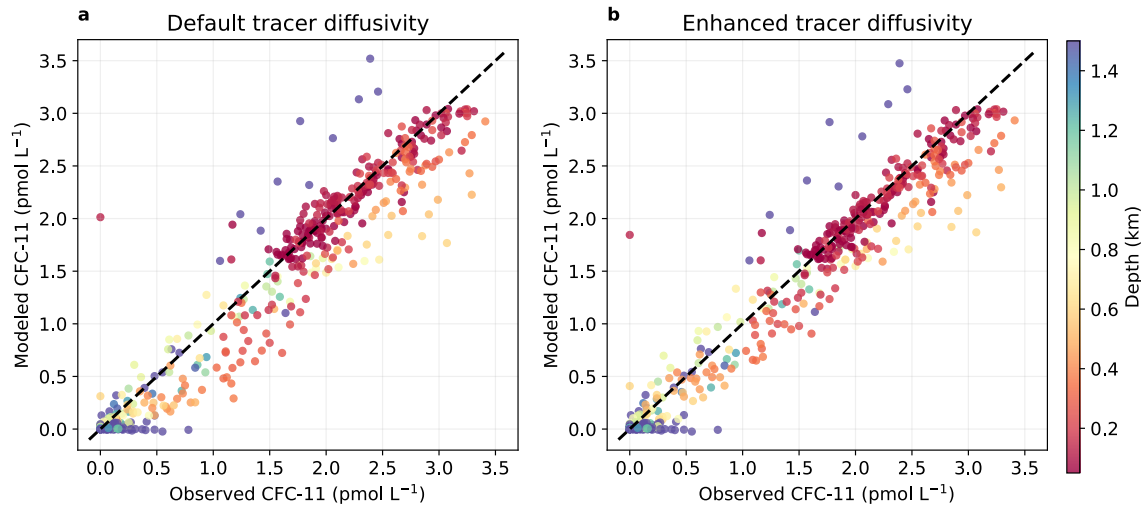


Figure S5. Testing ECCO tracer diffusivity using CFC-11 observations. Scatter plots of observed (x-axis) versus ECCO-simulated (y-axis) CFC-11 concentrations, co-located in space and time, color-coded by depth. Panel **a** uses the default tracer diffusivity in ECCO. Panel **b** enhances vertical tracer diffusivity in ECCO by adding constant $2 \times 10^{-5} \text{ m}^2 \text{ s}^{-1}$ between 65 m and 1,515 m depth. This enhanced tracer diffusivity leads to better agreement with observations, improving the coefficient of determination (R^2) from 0.90 to 0.93 above 1,500 m depth.

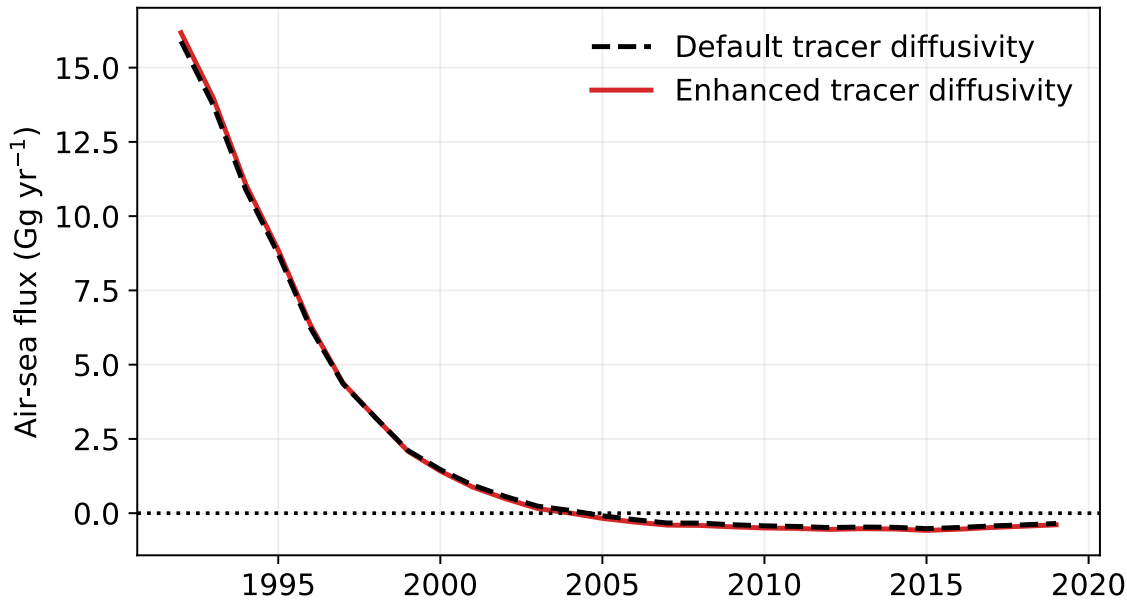


Figure S6. Effect of tracer diffusivity on MCF air-sea flux. The black dashed line shows the globally integrated MCF air-sea flux using the default ECCO tracer diffusivity, while the red solid line shows the result using an enhanced diffusivity by adding $2 \times 10^{-5} \text{ m}^2 \text{ s}^{-1}$ between 65 m and 1,515 m depth. This increase in tracer diffusivity has a minimal effect on the global air-sea flux of MCF.

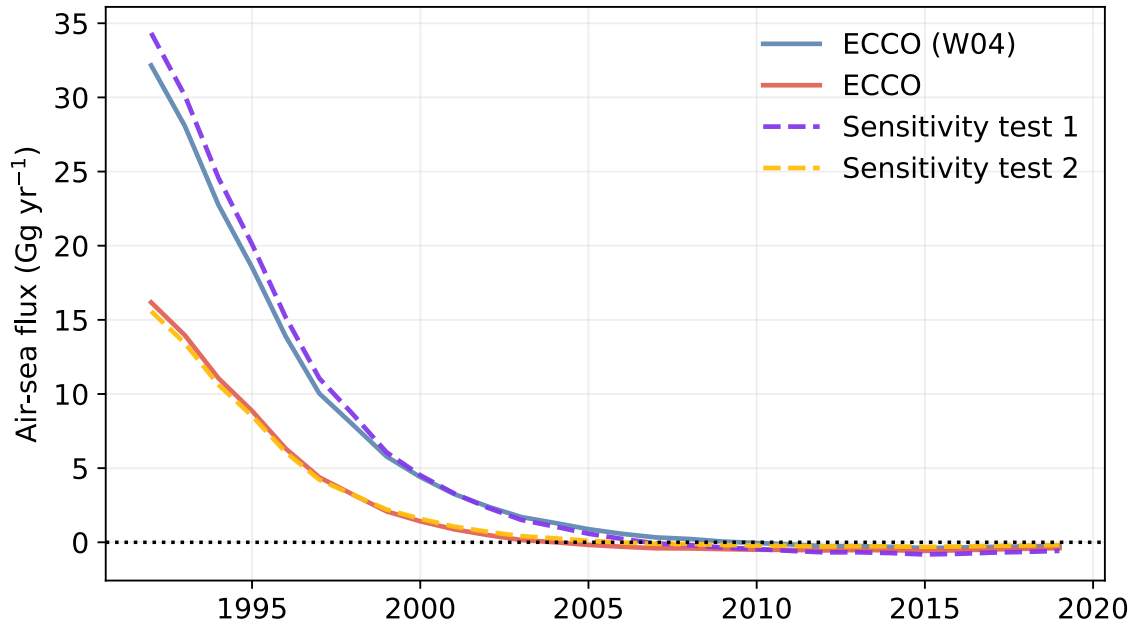


Figure S7. Sensitivity of MCF air-sea flux to solubility and hydrolysis parameters. The blue and red lines (same as in Figure 3) show the globally integrated air-sea flux of MCF from 1992 to 2019 in ECCO, using (blue) the same freshwater solubility and hydrolysis rate from W04, and (red) the seawater solubility and a slower cold-temperature hydrolysis rate. Two sensitivity tests were performed to isolate the effects of changing solubility and hydrolysis. Sensitivity test 1 (purple dashed line) considers freshwater solubility (as in W04) but with a slower cold-temperature hydrolysis rate. Sensitivity test 2 (yellow dashed line) considers seawater solubility but with the same hydrolysis rate as in W04. The comparison shows that switching from freshwater to seawater solubility is the dominant factor in reducing oceanic MCF uptake, resulting in earlier onset of ocean outgassing.

Table S1. Seawater solubility coefficients for CFC-11 (directly obtained from Warner & Weiss, 1985) and MCF (described in Supplementary Text S1). The coefficients are fitted to the polynomial $H_{sw} = \exp \left(A_1 + A_2 \left(\frac{100}{T} \right) + A_3 \ln \left(\frac{T}{100} \right) + A_4 \left(\frac{T}{100} \right)^2 + SB_1 + SB_2 \left(\frac{T}{100} \right) + SB_3 \left(\frac{T}{100} \right)^2 \right)$, where H_{sw} has units in mol atm⁻¹ L⁻¹, T is temperature in Kelvin, and S is salinity in g L⁻¹.

Coefficients	CFC-11	MCF
A ₁	-229.9261	-28.3913
A ₂	319.6552	55.63613
A ₃	119.4471	7.54752
A ₄	-1.39165	-0.14761
B ₁	-0.142382	0.2295
B ₂	0.091459	-0.12942
B ₃	-0.0157274	0.01477

References

- Butler, J. H., Elkins, J. W., Thompson, T. M., Hall, B. D., Swanson, T. H., & Koropalov, V. (1991). Oceanic consumption of CH₃CCl₃: Implications for tropospheric OH. *Journal of Geophysical Research: Atmospheres*, 96(D12), 22347–22355. <https://doi.org/10.1029/91JD02126>
- Forget, G., Ferreira, D., & Liang, X. (2015). On the observability of turbulent transport rates by Argo: supporting evidence from an inversion experiment. *Ocean Science*, 11(5), 839–853. <https://doi.org/10.5194/os-11-839-2015>
- Gerkens, R. R., & Franklin, J. A. (1989). The rate of degradation of 1,1,1-trichloroethane in water by hydrolysis and dehydrochlorination. *Chemosphere*, 19(12), 1929–1937. [https://doi.org/10.1016/0045-6535\(89\)90016-7](https://doi.org/10.1016/0045-6535(89)90016-7)
- Gossett, J. M. (1987). Measurement of Henry's law constants for C1 and C2 chlorinated hydrocarbons. *Environmental Science & Technology*, 21(2), 202–208. <https://doi.org/10.1021/es00156a012>
- Trossman, D. S., Whalen, C. B., Haine, T. W. N., Waterhouse, A. F., Nguyen, A. T., Bigdeli, A., et al. (2022). Tracer and observationally derived constraints on diapycnal diffusivities in an ocean state estimate. *Ocean Science*, 18(3), 729–759. <https://doi.org/10.5194/os-18-729-2022>
- Wanninkhof, R. (1992). Relationship between wind speed and gas exchange over the ocean. *Journal of Geophysical Research: Oceans*, 97(C5), 7373–7382. <https://doi.org/10.1029/92JC00188>
- Wanninkhof, R. (2014). Relationship between wind speed and gas exchange over the ocean revisited. *Limnology and Oceanography: Methods*, 12(6), 351–362. <https://doi.org/10.4319/lom.2014.12.351>
- Warner, M. J., & Weiss, R. F. (1985). Solubilities of chlorofluorocarbons 11 and 12 in water and seawater. *Deep Sea Research Part A. Oceanographic Research Papers*, 32(12), 1485–1497. [https://doi.org/10.1016/0198-0149\(85\)90099-8](https://doi.org/10.1016/0198-0149(85)90099-8)
- Wennberg, P. O., Peacock, S., Randerson, J. T., & Bleck, R. (2004). Recent changes in the air-sea gas exchange of methyl chloroform. *Geophysical Research Letters*, 31(16). <https://doi.org/10.1029/2004GL020476>